Article

Cell Reports

# Induction of an Alternative mRNA 5′ Leader Enhances Translation of the Ciliopathy Gene *Inpp5e* and Resistance to Oncolytic Virus Infection

## Graphical Abstract

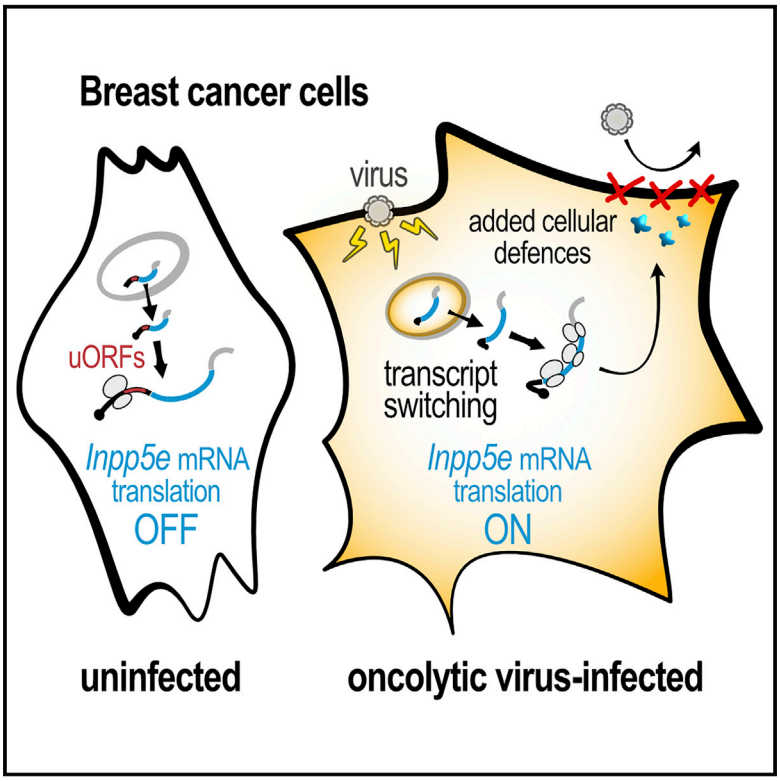


## Authors

Huy-Dung Hoang, Tyson E. Graber, Jian-Jun Jia, ..., Maritza Jaramillo, Seyed Mehdi Jafarnejad, Tommy Alain

## Correspondence

tommy@mgcheo3.med.uottawa.ca

## In Brief

Resistance of tumors to "oncolytic" viral therapies can be mediated by changes in cellular mRNA translation upon infection. Hoang et al. explore translatomes of infected breast cancer cells, identifying *Inpp5e* as a regulated viral resistance gene. In this context, transcript switching favors an *Inpp5e* mRNA variant with increased translational output.

## Highlights

- Oncolytic virus infection decouples transcription and translation in cancer cells
- Upstream ORFs (uORFs) repress translation of *Inpp5e* mRNA in uninfected cells
- Infection favors a translationally active *Inpp5e* variant lacking intronic uORFs
- *Inpp5e* knockout cells exhibit increased HSV1 attachment and infection

Hoang et al., 2019, Cell Reports *29*, 4010–4023
December 17, 2019 
https://doi.org/10.1016/j.celrep.2019.11.072

CellPress

OPEN ACCESS
CellPress

Cell Reports
Article

# Induction of an Alternative mRNA 5′ Leader Enhances Translation of the Ciliopathy Gene *Inpp5e* and Resistance to Oncolytic Virus Infection

Huy-Dung Hoang,[1,2,10] Tyson E. Graber,[1,3,10] Jian-Jun Jia,[1] Nasana Vaidya,[1] Victoria H. Gilchrist,[1,2] Xiao Xiang,[1,4] Wencheng Li,[5] Kyle N. Cowan,[1,4,6] Christos G. Gkogkas,[7] Maritza Jaramillo,[8] Seyed Mehdi Jafarnejad,[9] and Tommy Alain[1,2,11,*]

[1]Children's Hospital of Eastern Ontario Research Institute, Ottawa, ON K1H 8L1, Canada
[2]Department of Biochemistry, Microbiology, and Immunology, University of Ottawa, Ottawa, ON K1H 8M5, Canada
[3]Department of Biochemistry and Goodman Cancer Center, McGill University, Montreal, QC H3A 1A3, Canada
[4]Department of Cellular and Molecular Medicine, University of Ottawa, Ottawa, ON K1H 8M5, Canada
[5]Department of Biochemistry and Molecular Biology, Rutgers New Jersey Medical School, Newark, NJ 07101, USA
[6]Department of Surgery, Children's Hospital of Eastern Ontario, University of Ottawa, Ottawa, ON K1H 8L1, Canada
[7]Centre for Discovery Brain Sciences, University of Edinburgh, Edinburgh EH8 9XD, UK
[8]INRS Institut Armand-Frappier Research Centre, Laval, QC H7V 1B7, Canada
[9]Centre for Cancer Research and Cell Biology, School of Medicine, Dentistry and Biomedical Science, Queen's University Belfast, Belfast BT9 7AE, UK
[10]These authors contributed equally
[11]Lead Contact
*Correspondence: tommy@mgcheo3.med.uottawa.ca
https://doi.org/10.1016/j.celrep.2019.11.072

## SUMMARY

**Residual cell-intrinsic innate immunity in cancer cells hampers infection with oncolytic viruses. Translational control of mRNA is an important feature of innate immunity, yet the identity of translationally regulated mRNAs functioning in host defense remains ill-defined. We report the translatomes of resistant murine "4T1" breast cancer cells infected with three of the most clinically advanced oncolytic viruses: herpes simplex virus 1, reovirus, and vaccinia virus. Common among all three infections are translationally de-repressed mRNAs, including *Inpp5e*, encoding an inositol 5-phosphatase that modifies lipid second messenger signaling. We find that viral infection induces the expression of an *Inpp5e* mRNA variant that lacks repressive upstream open reading frames (uORFs) within its 5′ leader and is efficiently translated. Furthermore, we show that INPP5E contributes to antiviral immunity by altering virus attachment. These findings uncover a role for translational control through alternative 5′ leader expression and assign an antiviral function to the ciliopathy gene *Inpp5e*.**

## INTRODUCTION

Mammalian cells possess a sophisticated cell-intrinsic innate antiviral program that is activated upon infection. Transcriptional induction of type I interferon expression (IFN-α and -β) and downstream interferon-stimulated genes (ISGs) is a major arm of the innate immune response to infection (Schneider et al., 2014). Another essential feature of this response is the mRNA translation arm of innate immunity, a reprogramming of protein synthesis to permit the expression of cellular antiviral proteins while concurrently thwarting the production of viral proteins (Walsh et al., 2013).

Translation initiation can be modulated by several eukaryotic initiation factors (eIFs) and RNA-binding proteins (RBPs) (Sonenberg and Hinnebusch, 2009). In addition to the $m^7G$ cap structure, which helps recruit eIFs, other *cis*-acting sequence elements that lie within 5′ leaders, such as 5′ terminal oligopyrimidine (TOP) motifs, upstream open reading frames (uORFs), internal ribosome entry sites (IRESs), RBP binding sites, or localized secondary structure can govern the translational efficiency (TE) of mRNAs (Leppek et al., 2018; Shi and Barna, 2015). During infection, signaling cascades that feed into mRNA translation such as phosphatidylinositol 3-kinase (PI3K)/mammalian target of rapamycin complex 1 (mTORC1)/(S6K or 4E-BP) and ERK/MNK/eIF4E were shown to enhance the translation of antiviral mRNAs, including *IRF7* and *ISG15* (Colina et al., 2008; Zakaria et al., 2018). Conversely, translation initiation can be transiently suppressed following infection by preventing efficient ribosome assembly through the activation of eIF2α kinases and subsequent phosphorylation of the α subunit of eIF2 (P-eIF2α) (Hoang et al., 2018). In contrast, some cellular mRNAs that have uORFs (e.g., *ATF4*; Blais et al., 2004) and/or IRES (e.g., *cIAP1*/*BIRC2*; Graber et al., 2010) in their 5′ leaders display enhanced TE in conditions of high P-eIF2α. Alternative mRNA transcription, splicing, and polyadenylation can also indirectly modify translational output by altering 5′ leaders and 3′ UTRs, thus changing the composition of sequence elements that affect TE (Wang et al., 2016).

Viruses use a plethora of strategies to maximize TE of their own mRNAs, from evolving 5′ leaders that are better substrates for translation due to the presence of IRES to deploying proteins that shutdown global cellular translation (host shutoff) (Walsh et al., 2013). Surveying which cellular and viral mRNAs are

translated in this highly dynamic environment has been the subject of some recent studies (Dai et al., 2017; Tirosh et al., 2015). However, these investigations did not specifically address how the translation of mRNAs encoding putative pro- or antiviral effectors could modulate infection. Furthermore, the identification of host mRNAs under translational control during infection could provide targetable strategies to improve antiviral therapies or alleviate viral resistance, an undesirable feature of tumor cells in the context of oncolytic virus therapy, which represents a promising class of cancer therapeutics that relies on natural or engineered cancer cell tropism and mobilization of adaptive, anti-tumor immunity (Harrington et al., 2019).

In this work, we ask which mRNA substrates of translation contribute to the viral resistance of 4T1 breast cancer cells infected with each of three leading oncolytic viruses: herpes simplex virus 1-1716 (HSV1; Sorrento Therapeutics), reovirus type 3 Dearing (also called Reolysin; reovirus; Oncoytics Biotech), and vaccinia virus JX-594 (VACV; Sillajen). Comparing viral versus mock infected, we identify translationally upregulated host mRNAs common to all three infections. We show that the 5′ leaders of these mRNAs are enriched in uORFs and are translationally repressed in mock conditions but become derepressed upon infection. This subset includes mRNAs encoding proteins that are associated with primary cilium homeostasis. We characterize the important ciliopathy gene *Inpp5e*, encoding an inositol 5-phosphatase, and describe a virus-induced mRNA variant switch that releases its uORF-mediated translation repression. This response limits viral propagation as cells deficient in INPP5E exhibit increased cell surface attachment of virions and subsequent infection efficiency. These findings highlight the dynamic landscape of alternative 5′ leader usage during viral infection and identify INPP5E as a translationally induced antiviral effector that limits oncolytic virus efficacy.

## RESULTS

### Transcription and Translation Are Uncoupled in Response to Oncolytic Virus Infection of 4T1 Cells

To assess translationally regulated innate immune genes, we used HSV1, reovirus, and VACV individually to infect 4T1 cells, a murine mammary carcinoma model that is refractory to viral oncolysis and closely resembles stage IV human breast cancer. Each of these viruses has a different rate of infection that eventually results in the shutdown of host cell translation (Walsh et al., 2013). We therefore selected an effective dose that is cytopathic for 50% ($ED_{50}$) of 4T1 cells at 48 h post-infection (Figure 1A). At 18 h post-infection, polysome profiles (Figure 1B) and $^{35}$S-methionine labeling (Figure 1C) showed robust viral protein synthesis, while that of the host cells was only slightly affected. The majority of cells were infected at this dose and time point, confirmed by co-expression of a virion-derived GFP transgene in the case of HSV1 and VACV (Figure S1A).

We profiled both the transcriptome and translatome signatures of 4T1 cells, with each individual infection compared to mock-infected controls using the ribosome-profiling method (summarized in Figure 1D) (Ingolia et al., 2009). By in-parallel sequencing of ribosome-protected footprints (RPFs) and total mRNA (RNA), the ribosome occupancy and thus TE (RPF/RNA) of individual mRNA species was quantitated. In contrast to total RNA read densities, which were constant throughout the exonic regions, RPF densities were found to increase within annotated coding sequences (CDSs) relative to 5′ leaders and 3′ UTRs, which is consistent with ribosomes engaged in translation (Figure S1B). Regression analysis of reads normalized to CDS length and sequencing depth (reads per kilobase of CDS per million reads sequenced [RPKM]) in two biological replicates showed a high degree of correlation at both the RNA (i.e., transcriptome) and the RPF (i.e., translatome) genomic levels (Figure S1C). These data demonstrate that ribosome profiling successfully captured the transcriptional and translational states of the 4T1 genome following challenge with three distinct oncolytic viruses.

We next determined the differentially expressed genes (DEGs) at the transcriptome and translatome levels in virus- versus mock-infected 4T1 cells (Table S1). We used a cutoff of 1.5-fold change in expression up or down and found that reovirus modified transcript abundance to a higher degree (24% of sequenced genes) than HSV1 (5.7%) or VACV (1.5%) (Figure 1E, top). In stark contrast, TEs were perturbed more consistently between all three viruses: reovirus (18% of sequenced genes), VACV (12%), and HSV1 (15%) (Figure 1E, bottom). We also found a poor correlation between the transcriptome and the translatome (Pearson's correlation coefficients of 0.46, 0.20, and 0.24 for reovirus, VACV, and HSV1 versus mock, respectively) (Figure 1F). Thus, changes in the transcriptional profile of any given gene is a poor predictor of its TE, a finding that has been replicated in other experimental contexts (Schwanhäusser et al., 2011; Tebaldi et al., 2012).

### Genes of the Common Translatome between All Three Infections Function in Pathways Not Previously Associated with Viral Infections

A primary objective of this study was to identify innate immunity effectors that could function in a general antiviral program during any of the three infections. To this end, we determined the set of DEGs common to all three infections at both the transcriptome and the translatome levels (Figure 2A; Table S2). We performed Gene Ontology (GO) functional enrichment analysis on these shared sets and found the expected functional groups at the transcriptional level, including terms encompassing pattern recognition signaling, response to infection, inflammatory response, and nucleic acid binding (Figure 2B). Of note, many previously validated ISGs (Schoggins et al., 2011) were found to be uniquely upregulated at the level of transcription with reovirus, VACV, or HSV1 infection, respectively (Figure S2A). Moreover, these ISGs populated 38% (13/34) of the transcriptionally upregulated DEGs common to all three infections (Figure S2B).

Functional enrichment at the level of the common translatome was found to be very different, with few specific GO terms. Translationally downregulated genes fell into categories encompassing catabolic and developmental cellular functions, while the upregulated common set was found to be enriched in genes involved in microtubule organization and the primary cilium, an organelle with a unique cytoskeleton and subcellular proteome that is often referred to as the cell's signaling antenna (Boldt et al., 2016) (Figure 2C; Table S3). Confirming the GO analysis,

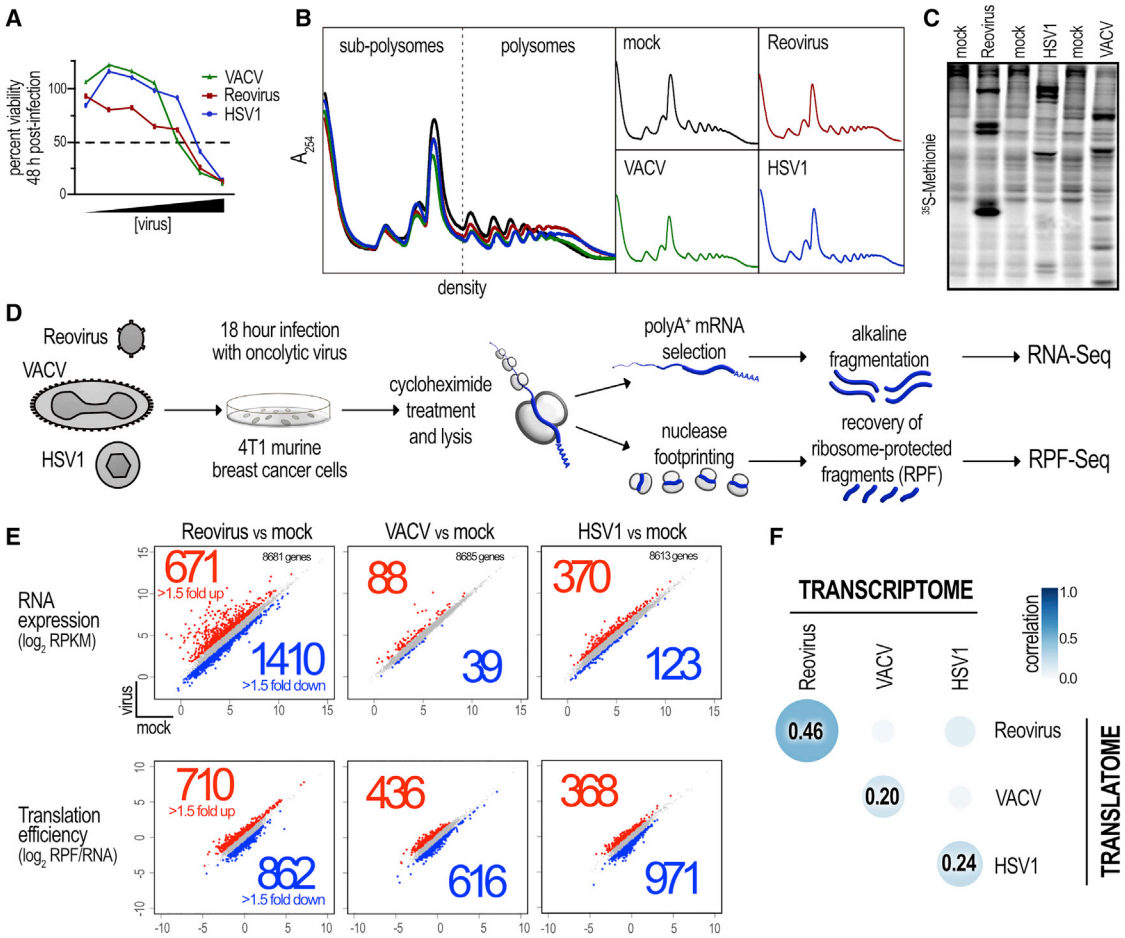


**Figure 1. Transcription and Translation Are Uncoupled in Response to Oncolytic Virus Infection of 4T1 Cells**

(A) Infectious dose-response viability curves for the three different viruses used in this study in murine 4T1 breast carcinoma cells.

(B and C) Polysome profiles of virus-infected versus mock-infected 4T1 cells at 18 h post-infection (B) and metabolic labeling with $^{35}$S-methionine followed by SDS-PAGE to resolve nascent peptides (C).

(D) Schematic illustration of the ribosome-profiling strategy used in this study.

(E) Differential expression of sequenced genes (total number shown in top right of plots) at both the transcriptional and the translational genome levels. Each point on the plots represent the average RNA expression or TE from two biological replicates. Genes that were up- (red) or downregulated (blue) >1.5-fold were considered to be differentially expressed.

(F) Correlation analysis of RNA-normalized (transcriptome) and RPF-normalized (translatome) abundance between viruses (all relative to mock infected). Pearson's correlation coefficients are presented.

there was significant enrichment ($p = 1.25 \times 10^{-4}$) of genes encoding proteins that constitute the ciliary interactome (Figure 2D) (Boldt et al., 2016). Thus, using ribosome profiling, the anticipated transcriptional but unexpected translational signatures of the antiviral state in oncolytic virus-infected 4T1 were obtained. This suggests that viral infection engenders a distinctive reprogramming of cellular translation.

## Oncolytic Viruses De-repress Translation of Host mRNAs Enriched in uORFs

To characterize the mode of control exerted on the translationally regulated transcripts, we looked for enrichment of RNA-binding protein motifs and microRNA (miRNA) target sequences (Figures S3A and S3B). We also surveyed the GC content of these annotated transcripts as well as the lengths of their 5′ leaders, CDSs, and 3′ UTRs, comparing them to all NCBI Reference Sequence (RefSeq) mouse mRNAs. While we found no significant difference in GC content, the shared translationally regulated mRNAs (either up- or downregulated) tended to have shorter 5′ leaders, CDSs, and 3′ UTRs (Figure 3A). In analyzing the distribution of TEs for the commonly upregulated set of genes, we noted that this subset was dramatically repressed in mock-infected cells compared to the entire sequenced set (Figure 3B; compare "mock" distributions). This property appeared to be mainly due to lower RPF expression in the upregulated genes (Figure S3C, center). Viral infection acted to significantly de-repress the translation of these genes independently of changes at the RNA level (Figure 3B, shift in distribution denoted by arrow, and Figure S3C, right). In contrast, the downregulated set of genes followed a mock-infected TE distribution profile that

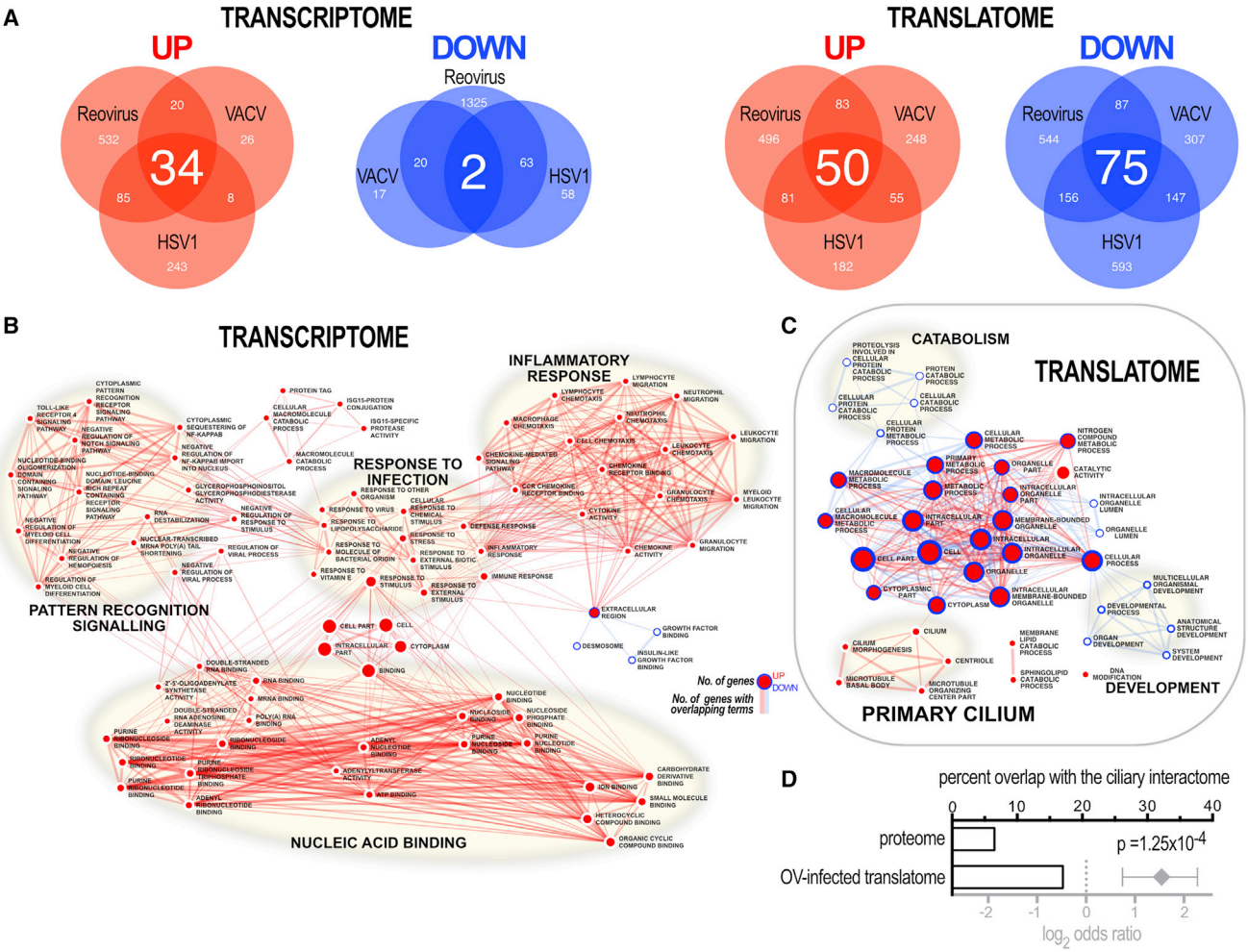


**Figure 2. Genes of the Common Translatome between All Three Infections Function in Pathways Not Previously Associated with Viral Infections**

(A) Venn diagrams illustrating the common and unique sets of DEGs between viral infections at transcriptional and translational levels.

(B) Network analysis of enriched GO terms for the DEGs commonly regulated by all three oncolytic viruses at the transcriptional level. Generic terms are concentrated at the center and specific terms lie at the extremities. Node diameter and edge thickness are proportional to the number of genes belonging to or overlapping with GO terms, respectively.

(C) As in (B), except at the level of the translatome.

(D) Percentage of the human proteome ("proteome"; 1,319/20,195 proteins) versus the percentage of orthologous genes in the common up and down 4T1 translatomes (OV-infected translatome; 19/112) that overlap with the ciliary interactome (Boldt et al., 2016). A Fisher's exact test was used to determine statistical significance. The odds ratio is presented with bars representing a 95% confidence interval and indicating an overrepresentation of ciliary proteins in the OV-infected translatome.

was indistinguishable from the entire set of sequenced genes that shifted to lower TE upon viral infection (Figure 3B, right, denoted by arrow). Furthermore, a similar analysis performed on the upregulated gene sets uniquely associated with each of the three viruses showed no clear de-repression profile, suggesting that this property is a specific and common cellular response to different viral infections (Figure 3C, top). Downregulated members of virus-unique sets behaved similarly to the shared set with respect to their TE distributions (Figure 3C, bottom).

This repression/de-repression profile has previously been ascribed to *cis*-acting mechanisms of translational control involving uORFs. We used an empirically derived list of uORF-containing mouse and human mRNAs (Lee et al., 2012) and found an overrepresentation in the commonly upregulated set, while no enrichment was seen for the downregulated set (Figure 3D). Thus, three different viruses were found to commonly affect the translation of transcripts whose 5′ leaders are more likely to contain uORFs, suggesting a universal cellular response to viruses that target cellular mRNAs harboring uORFs.

## INPP5E Is Translationally Induced during the Host Antiviral Response

We next aimed to validate the increased TE of the primary cilium genes identified in the network analysis. One of these included the

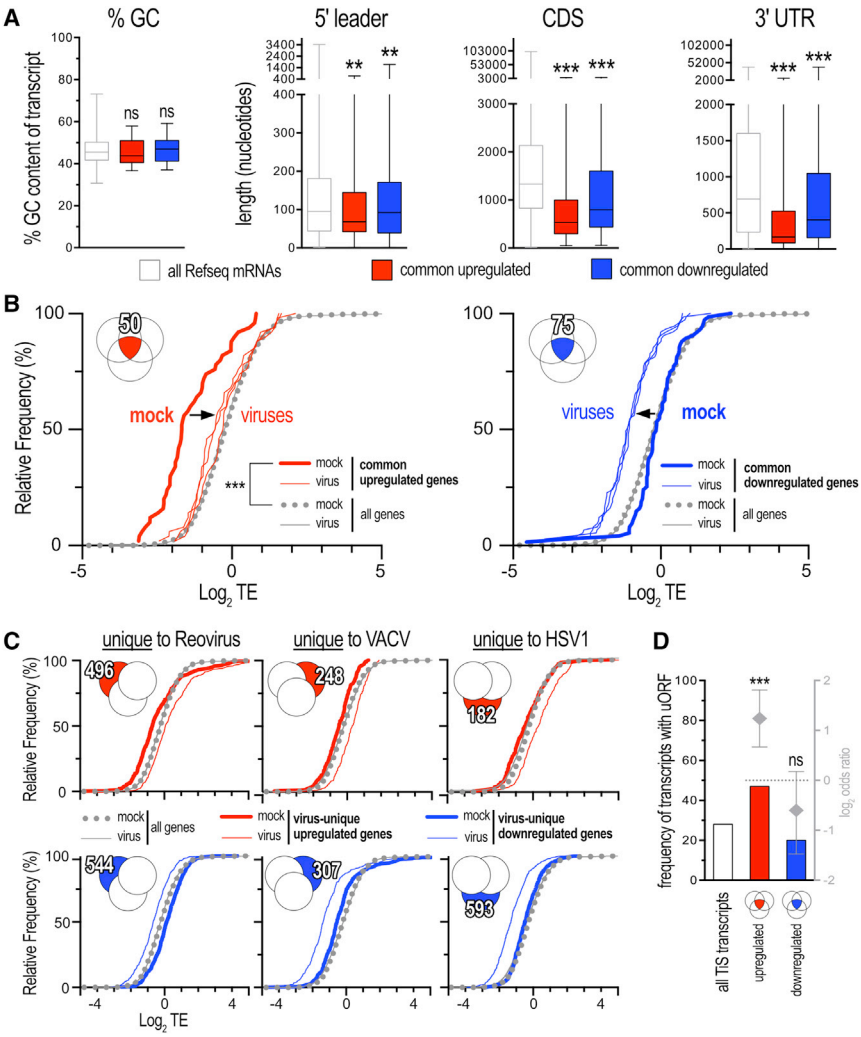


**Figure 3. Oncolytic Viruses De-repress Translation of Host mRNAs Enriched in uORFs**

(A) Analysis of RefSeq mRNA sequence characteristics that populate the common translationally regulated gene sets (red or blue bars) compared to the entire RefSeq database (white bars, see STAR Methods for details). Statistical significance was determined using Kruskal-Wallis with Dunn's post hoc testing,

(B) Relative frequency distributions of TE for common upregulated (left) versus downregulated (right) genes show that the former are translationally de-repressed (directional shifts indicated by an arrow). A Mann-Whitney statistical test was used.

(C) Analysis as in (B), but for the translationally regulated gene sets that are unique to each virus.

(D) Frequency of uORFs in all mouse and human transcripts in the TiS database (7,361/26,735; http://tisdb.human.cornell.edu) compared to that present in the translationally upregulated (52/110) and downregulated (17/85) sets of transcripts common to all 3 infections. The increased frequency of uORFs in the commonly upregulated set was found to be significant by Fisher's exact test, with the odds ratios presented with bars representing a 95% confidence interval, indicating overrepresentation of uORF-containing transcripts in the upregulated gene set. **p<0.01, ***p<0.001, ns, non-significant.

ciliopathy gene *Inpp5e*, an inositol 5-phosphatase linked to Joubert syndrome (Nachury et al., 2007). We reasoned that as *Inpp5e* TE is induced during virus infection, the double-stranded RNA (dsRNA) mimic poly(I:C) that induces an antiviral state via activation of IFN regulatory factor 3 (IRF3) and nuclear factor κB (NF-κB) should be able to recapitulate this control of INPP5E expression. While barely detectable in 4T1 cells in control conditions, immunofluorescence (IF) staining of INPP5E notably increased upon poly(I:C) treatment (Figure 4A, quantified in Figure 4B), yet *Inpp5e* mRNA abundance trended lower following the same treatment (Figure 4C). Consistent with the ribosome-profiling results, we observed that INPP5E protein measured by IF in wild-type 4T1 cells ($Inpp5e^{+/+}$) appeared at low levels in mock conditions but is robustly induced upon VACV infection (Figure 4D, quantified in Figure 4E). To confirm the specificity of the IF signal, we turned to CRISPR/Cas9 technology to generate two clones of 4T1 cells depleted of INPP5E ($Inpp5e^{CRISPR\#1}$, $Inpp5e^{CRISPR\#2}$). Tracking of indels by decomposition (TIDE) analysis (Brinkman et al., 2014) determined that the *Inpp5e* locus was modified at a frequency close to 100% with a mixture of three indels that would be predicted to disrupt expression (Figures S4A–S4C). The VACV-mediated induction of INPP5E protein seen in wild-type cells was lost in $Inpp5e^{CRISPR\#1}$ cells, despite a robust infection marked by strong GFP expression (Figure 4D, quantified in Figure 4E). Again, consistent with a post-transcriptional effect, total mRNA levels of *Inpp5e* were unaffected with VACV infection at similar MOI and time point (Figure 4F). HSV1 gE protein acts as an Fc receptor and binds immunoglobulin G (IgG) of various host species (Johansson et al., 1985), which we used as secondary antibodies for IF detection. Thus, we could not use IF to determine whether HSV1 caused a similar induction of INPP5E. We instead used western blotting and observed a band (with an apparent molecular weight of 62 kDa) induced with HSV1 infection in 4T1 cells (Figures 4G and S4D). Similar to the VACV data, we found that the HSV1-specific signal was lost in $Inpp5e^{CRISPR\#1}$ cells, despite a similar expression of HSV1 protein ICP0, indicating specificity for INPP5E (Figure S4D). The induction of INPP5E occurred in another cancer cell line, the mouse glioblastoma CT2A (Figure 4G). As was the case for either poly(I:C) or VACV treatments, *Inpp5e* mRNA abundance was not affected by HSV1 infection in either 4T1 or CT2A cells (Figure 4G).

The above data argue for the post-transcriptional regulation of *Inpp5e* in these contexts; however, post-translational changes such as increased protein stability may explain the increased expression of INPP5E with infection. We therefore determined the TE of *Inpp5e* mRNA using conventional polysome profiling, in

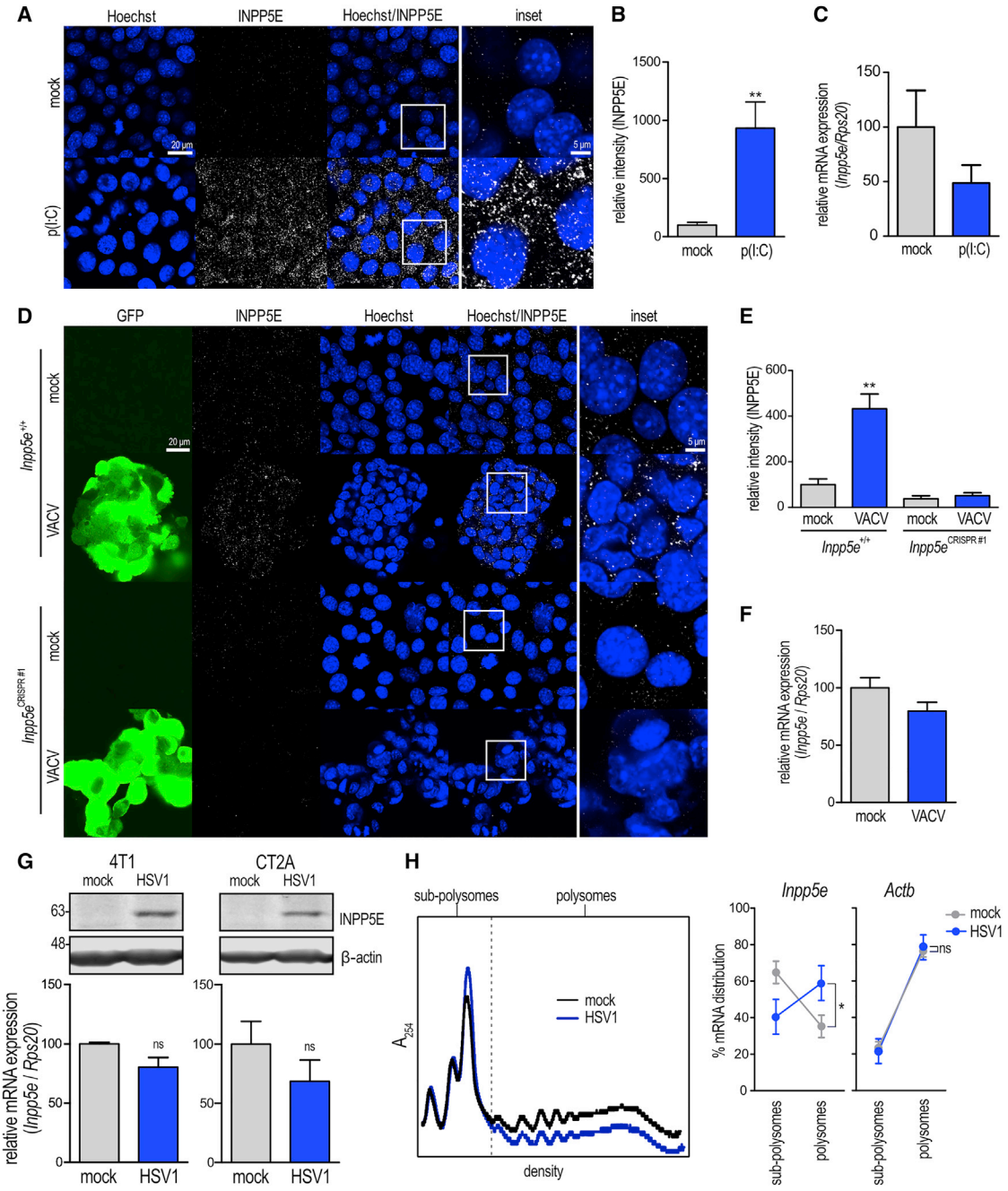


**Figure 4. INPP5E Is Translationally Induced during the Host Antiviral Response**

(A) Representative confocal images of anti-INPP5E stained 4T1 cells treated with poly(I:C) at 5 μg/mL or vehicle for 18 h.

(B) Quantification of the INPP5E IF signal in (A) normalized to mock.

(C) qRT-PCR of *Inpp5e* normalized to *Rps20* mRNA abundance in mock- or poly(I:C)-treated 4T1 cells for 18 h.

(D) As in (A), comparing INPP5E expression in mock-infected *Inpp5e*$^{+/+}$ or *Inpp5e*$^{CRISPR\#1}$ 4T1 cells or cells infected with VACV at 5 MOI.

(E) Quantification of the INPP5E IF signal in (D) (normalized to mock-infected cells).

(F) qRT-PCR of *Inpp5e* mRNA in mock-infected or VACV-infected 4T1 cells at 5 MOI for 24 h.

(G) Top: representative western blots of steady-state INPP5E protein expression in mock-infected and HSV1-infected 4T1 or CT2A cells at 18 h post-infection at 1 MOI. β-Actin is included as a loading control. Apparent molecular weights are indicated to the left in kilodaltons. Bottom: qRT-PCR of *Inpp5e* normalized to *Rps20* mRNA abundance in mock-infected or HSV1-infected cells at 24 h post-infection at 5 MOI in 4T1 and CT2A cells.

(H) Left: representative polysome profiles of mock-infected and HSV1-infected CT2A cells 4 h post-infection at MOI of 5. Right: distribution of *Inpp5e* and *Actb* mRNAs across sub-polysomes (low TE) and polysomes (high TE) in mock-infected versus HSV1-infected samples.

Error bars indicate standard error of the mean (sem). *$p < 0.05$, **$p < 0.01$, ns, non-significant, calculated using two-tailed t test.

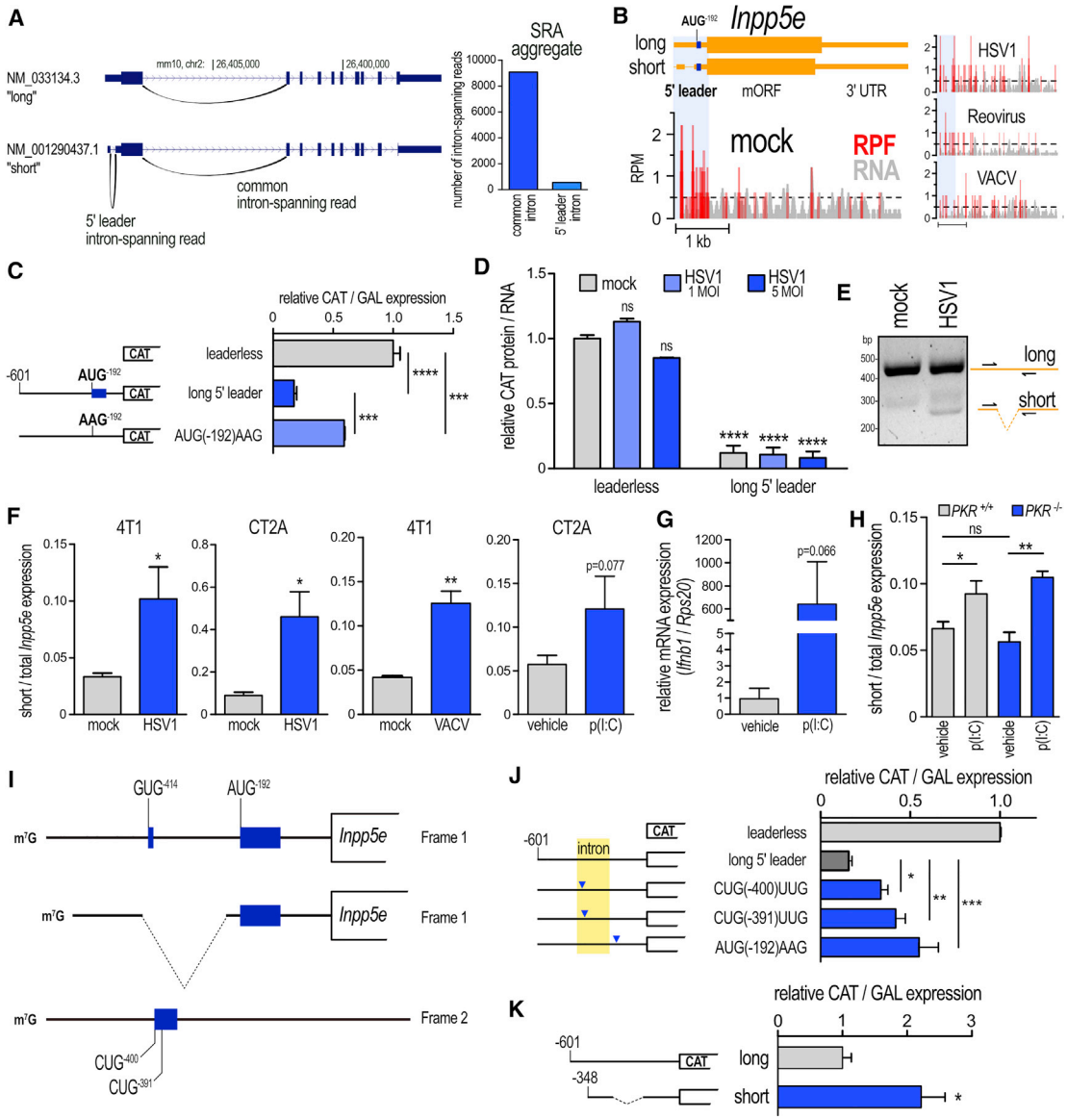


**Figure 5. Expression of an Alternative 5′ Leader during Infection Releases *Inpp5e* from uORF-Mediated Translational Repression**

(A) RefSeq-annotated *Inpp5e* transcripts showing "long" and "short" variants. RefSeq accessions are indicated. Deep sequencing reads were aggregated from a pool of samples in the Sequencing Read Archive (SRA; NCBI *Mus musculus* Annotation Release 106) and plotted (right) based on intron-spanning reads from the short 5′ leader intron or the first intron common to both transcripts.

(B) Chromatogram of read densities (reads per million [RPM]) merged from the two biological replicates of ribosome profiling in this study for the *Inpp5e* locus at both RNA and RPF gene expression levels showing a shift in RPF reads from the 5′ leader to the mORF following infection.

(C) Translation reporter assay in 4T1 cells showing that the long *Inpp5e* 5′ leader strongly represses the translation of the CAT ORF. Constructs used are pictured to the left and were co-transfected with a β-galactosidase (GAL) reporter to normalize any differences in transfection. The long leader-mediated repression is substantially weakened with a single mutation that abolishes a uORF start codon (AUG[−192]AAG) demonstrating a bona fide uORF mechanism of translational regulation.

(D) Translation reporter assay as in (C), but in 4T1 cells transfected with *in vitro* transcribed CAT RNA evaluated at 18 h post-HSV1 infection; n = 2 biological replicates.

(E) Agarose gel with resolved PCR amplicons from a 4T1 cDNA library indicates the expression of both the short and long *Inpp5e* 5′ leaders in HSV1-infected cells (a single set of primers flank the 5′ leader intron, pictured at right).

(F) qRT-PCR of short versus total *Inpp5e* mRNA showing an increased expression of the short variant with HSV1 infection after 48 h of infection in either 4T1 or CT2A cells, and VACV-infected 4T1 at 24 h post-infection or poly(I:C)-treated CT2A for 18 h.

(G) qRT-PCR of *Ifnb1* normalized to *Rps20* mRNA expression in CT2A cells treated with poly(I:C) for 18 h.

(H) Poly(I:C)-mediated induction of the short *Inpp5e* variant is PKR independent. Poly(I:C) 8 μg/mL was transfected into $PKR^{+/+}$ or $PKR^{-/-}$ MEFs, and short versus total *Inpp5e* RNA levels were determined by qRT-PCR 18 h later. A two-way ANOVA with Sidak post hoc test was used to determine significance.

*(legend continued on next page)*

which mRNAs are resolved based on the number of associated ribosomes. HSV1 infection (MOI of 5) was found to slightly but consistently reduce global mRNA translation at 4 h post-infection (Figure 4H, left). Unlike *Actb* mRNA, the majority (~80%) of which was found in the polysome fraction in uninfected CT2A cells, *Inpp5e* resided mainly (~60%) in sub-polysomes, which is indicative of a repressed translation state and consistent with the lack of observable protein seen in our IF and western blotting experiments (Figure 4H, right). However, the distribution of *Inpp5e* in active polysomes positively shifted from 35.24% ± 6.12% to 59.21% ± 9.53% between mock- versus HSV1-infected cells, while that of *Actb* did not change appreciably (76.49% ± 3.2% and 78.47% ± 6.8%, respectively). Thus, these data demonstrate that *Inpp5e* mRNAs, which are translationally repressed in basal conditions, are under positive translational control during viral infection in cancer cells, despite a general repression of global translation.

## Expression of an Alternative 5′ Leader during Infection Releases Inpp5e from uORF-Mediated Translational Repression

Our data demonstrated that *Inpp5e* translation is normally repressed in 4T1 and CT2A cells, as evidenced by its low TE in mock-infected cells from ribosome profiling, polysome profiling, and the low steady-state protein expression observed by western blotting and IF. Furthermore, the same assays showed that viral infection de-represses *Inpp5e* translation. We therefore hypothesized that this repression/de-repression shift is due to uORF-dependent translational control. There are "long" and "short" mouse *Inpp5e* mRNA variants with long and short 5′ leaders, respectively. The short leader results from a downstream alternative transcription start site (altTSS) and alternative splicing, removing an intron that lies entirely within the 5′ leader. Moreover, the short transcript is predicted to encode a C-terminally truncated protein isoform and is supported in the Sequence Read Archive (SRA) by intron-spanning reads that account for ~5% of all *Inpp5e* transcripts (Figure 5A), as well as a single RIKEN clone isolated from neonatal kidney tissue.

A previous genome-wide study of initiating ribosomes listed a putative uORF in both the long and short *Inpp5e* 5′ leaders (Figure 5B, top schema shows the long and short *Inpp5e* mRNA variant with the location of the putative uORF in dark blue) (Lee et al., 2012). Critically, in uninfected 4T1 cells, RPF read densities were concentrated in the *Inpp5e* leader region (Figure 5B, leader region highlighted in light blue). This density shifted to the main ORF (mORF) upon HSV1, reovirus, or VACV infections, which is strongly suggestive of a regulatory uORF.

To determine the presence of a bona fide uORF, we constructed a heterologous DNA reporter plasmid consisting of the long (601 nt) *Inpp5e* leader inserted in front of an mORF encoding chloramphenicol acetyl transferase (CAT) (Graber et al., 2010). We found that the long *Inpp5e* leader confers a very strong repressive effect onto CAT expression, with levels approaching only 20% of that observed in 4T1 cells transfected with a leaderless construct (Figure 5C). Mutating the methionine-coding AUG start codon of the putative uORF at −192 nt (uORF$^{-192}$; present in both long and short leaders) to AAG rescued CAT expression to ~60% of the leaderless construct (Figure 5C). These data show that *Inpp5e* leaders harbor a uORF whose translation represses that of the downstream cistron. This likely explains why this transcript is normally repressed at the level of translation, as seen in the ribosome and polysome profiling experiments.

We next tested whether *Inpp5e* uses a classical uORF de-repression mechanism to modulate its translation during viral infection. In this model, translation of uORF$^{-192}$ would dominate the mORF in basal conditions, while the inverse would prevail with viral infection. However, 4T1 cells transfected with *in vitro* synthesized, capped, and polyadenylated CAT reporter RNA showed no changes in *Inpp5e* leader-dependent translation with HSV1 infection even at high MOI (Figure 5D). Thus, we were unable to demonstrate that the induction of *Inpp5e* translation during viral infection uses a classical uORF de-repression mechanism.

An alternative possibility is that infection induces a shift in 5′ leader expression, potentially favoring the short variant of *Inpp5e*. By virtue of its lower 5′ leader complexity, this transcript could conceivably display increased TE. In support of this idea, we observed a decrease in the *Inpp5e* 5′ leader:CDS ratio of RNA read densities during virus infection, suggesting a shift in expression to the short 5′ leader variant (Figure S5A). Using the mixture of isoforms (MISO) algorithm (Katz et al., 2010), we also found a more generalized alteration of the splicing landscape during infection with each of the three viruses. We detected 195, 229, and 289 differentially spliced events in reovirus-infected, VACV-infected, or HSV1-infected versus mock-infected 4T1 cells, respectively (Figures S5B and S5C). However, MISO was unable to call differentially spliced events in the list of shared translationally regulated genes, potentially due to their low mapping density, as most were found to be rarer mRNAs (Figure S3C, left).

To monitor the expression of the short and long variants, we designed PCR primers to flank the intron in the 5′ leader and could readily detect the long variant in either mock- or HSV1-infected 4T1 cells, while the short variant was evident only in the latter condition (Figure 5E). We next repeated the experiment in both 4T1 and CT2A cells using qRT-PCR primers designed to span the exon-exon junction of the short 5′ leader and found that the short variant in uninfected 4T1 or CT2A cells represented 3.32% ± 0.325% and 8.89% ± 1.53%, respectively, of the total

(I) Schematic of the *Inpp5e* 5′ leader region in both the long (top) and short (center) mRNA transcript variants in reading frame 1, which encodes INPP5E, and frame 2, which is non-coding (bottom). Putative start codons are indicated, with numbering relative to the first A of the *Inpp5e* AUG start codon in the long variants. Locations of potential uORFs are indicated with dark blue rectangles.

(J) CAT reporter assays were performed as in (C) with uORF start codon mutations (CUG[−400]UUG, CUG[−391]UUG, AUG[−192]AAG; indicated by blue triangles) in the long *Inpp5e* 5′ leader construct.

(K) Translation reporter assay of DNA-transfected 4T1 cells showing that the short *Inpp5e* 5′ leader variant (348 nt) is a markedly better substrate for translation than the long 5′ leader variant (601 nt).

Error bars indicate standard error of the mean (sem). *$p < 0.05$, **$p < 0.01$, ***$p < 0.001$, ****$p < 0.0001$, ns, non-significant, calculated using two-tailed t test.

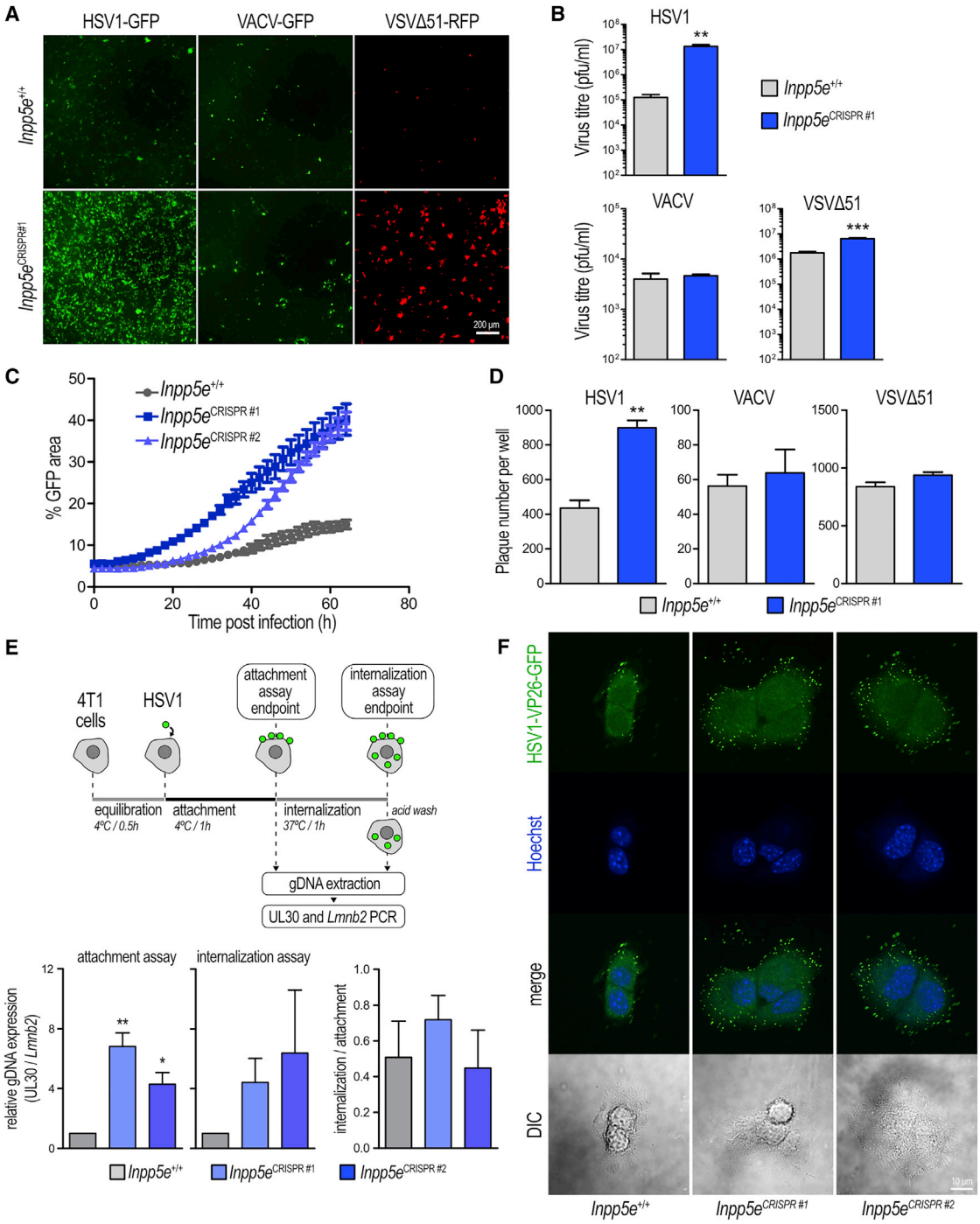


**Figure 6. INPP5E Acts as an Antiviral Effector That Modifies Viral Binding**

(A) Representative fluorescence microscopy images of virus infections at MOI of 0.1 for 24 h (VSVΔ51-RFP) or 48 h (HSV1-GFP and VACV-GFP) in *Inpp5e*$^{CRISPR\#1}$ versus *Inpp5e*$^{+/+}$ 4T1 cells.

(B) Titration of virus obtained from the supernatant of *Inpp5e*$^{CRISPR\#1}$ versus *Inpp5e*$^{+/+}$ 4T1 cells infected with the indicated viruses at 0.01 MOI for 24 h (VSVΔ51-RFP) or 48 h (HSV1 and VACV).

(C) Live-cell measurements of HSV1-GFP infection in both *Inpp5e*$^{CRISPR}$ clones compared to control 4T1. Cells were infected at an MOI of 0.1 and images were taken every 2 h.

(D) Plaque assay in indicated CRISPR cells. Cells were infected with VSVΔ51, HSV1, and VACV at an MOI of 0.01, then plaques were enumerated from full-well fluorescence microscopy images.

*(legend continued on next page)*

abundance of *Inpp5e* mRNA (total *Inpp5e* was detected with primers annealing to a 3′ exon common to both the long and short transcripts) (Figure 5F). Infection with HSV1 caused a significant increase in the expression of the short variant relative to total *Inpp5e* mRNA levels to 10.19% ± 2.8% and 46.08% ± 11.74% in 4T1 and CT2A, respectively (Figure 5F). Similarly, VACV infection elevated the short:total *Inpp5e* mRNA ratio from 4.2% ± 0.00037% to 12.5% ± 0.014% in 4T1 cells (Figure 5F). Moreover, poly(I:C) treatment was also found to consistently enhance short variant expression in CT2A at 8 h post-treatment (Figure 5F), concomitant with a robust induction *Ifnb1* mRNA expression, which is indicative of a typical response to the dsRNA mimic (Figure 5G). Protein kinase R (PKR) activation has been previously shown to modulate mRNA splicing (Ilan et al., 2017); therefore, we asked whether induction of the short *Inpp5e* variant was dependent on this kinase. Although we could recapitulate the poly(I:C)-mediated induction of the short variant in wild-type mouse embryonic fibroblasts (MEFs), there was a similar induction in their PKR null counterparts, suggesting that induction of this short variant is PKR independent (Figure 5H).

We reasoned that there may be other uORFs in the 5′ leader intronic region that repress the translation of the mORF and are spliced out during viral infection. Two other ribosome-profiling studies in lipopolysaccharide-treated dendritic cells (Fields et al., 2015) and SOX-treated keratinocytes (Sendoel et al., 2017) showed relatively strong initiating ribosome peaks at two near-cognate CUG start codons at 400 and 391 nt upstream of the main CDS, respectively (referred to here as $CUG^{-400}$ and $CUG^{-391}$) (Figure S5D, upper blue track). In addition, elongating ribosome footprints are abundant in the 5′ leader, which is suggestive of active uORF translation (Figure S5D, lower red track). The putative uORFs starting at $CUG^{-400}$ and $CUG^{-391}$ are 141 and 132 nt in length, respectively, and in-frame with each other but out-of-frame with the other uORFs and the mORF (Figure 5I). To determine whether these codons are used to initiate the translation of bona fide uORFs, we mutated each of them in the *Inpp5e* long leader CAT construct and determined CAT expression. Mutating the −400 or −391 CUG codon to UUG resulted in a significant enhancement in CAT expression in either construct (Figure 5J). Thus, near-cognate CUG start codons in the 5′ leader intron contribute to uORF-mediated repression of *Inpp5e* translation.

Finally, we asked whether the short *Inpp5e* transcript variant is a better substrate for translation. Comparison of CAT expression in transfected 4T1 cells revealed that the short (spliced) 5′ leader confers a 2-fold enhancement of CAT expression relative to the long (unspliced) 5′ leader (Figure 5K). These data expound a complex expression profile for *Inpp5e*; repressive uORFs prevent the inappropriate translation of *Inpp5e* under normal conditions but are removed following viral infection to enhance its translation.

## INPP5E Functions as an Antiviral Effector That Modifies Viral Binding

We next investigated the potential function of INPP5E in modulating viral infection using our $Inpp5e^{CRISPR}$ cells. These cells exhibited an increased expression of virally expressed GFP following HSV1 infection relative to wild-type 4T1 cells (Figure 6A). Infection with VSVΔ51 (a negative-sense, single-stranded RNA oncolytic virus candidate) was also enhanced in $Inpp5e^{CRISPR}$ cells, although no clear difference was observed with VACV (Figure 6A). In addition, we knocked down *Inpp5e* expression in CT2A cells using a short hairpin RNA (shRNA) and found an increase in HSV1 protein expression relative to cells expressing non-targeting shRNA (shNTC) (Figure S6A).

To confirm the microscopy results, we quantified the production of infectious virus particles in the media of infected $Inpp5e^{CRISPR}$ 4T1 cells. Cells lacking INPP5E exhibited a 2-log increase in HSV1 viral particle production compared to $Inpp5e^{+/+}$ 4T1 cells (Figure 6B). Although we observed consistent increases in fluorescence with VSVΔ51 by microscopy, there was only a small but significant increase in viral titer (~5-fold increase, $p < 0.001$) and no significant change was observed in VACV titers, suggesting that the INPP5E effect in curtailing infection may be virus specific. Notably, RNA-mediated reduction in BBS9, another ciliary protein under translational control in our screen, also rendered 4T1 cells more permissive to viral infection (Figures S6B and S6C). In contrast, decreasing the expression of two translationally downregulated genes, *Usp18* and *Usp44*, compromised HSV1 infectivity (Figures S6D and S6E), suggesting that not only are antiviral genes translationally upregulated but also potential proviral genes are downregulated as part of a concerted effort by the host to quash infection.

To determine the stage(s) of the viral life cycle that could be affected by *Inpp5e*, we examined whether $Inpp5e^{CRISPR}$ cells could support increased viral spread. We infected cells with HSV1-GFP at low MOI (0.1) and measured GFP intensity and area every 2 h using a live-cell-imaging system. By quantitating the area of GFP signal in infected clusters normalized to the total imaged surface area at multiple time points, a more pronounced spread in the two $Inpp5e^{CRISPR}$ 4T1 cell lines compared to the control cell line was observed (Figure 6C). We found that this INPP5E-mediated effect on viral infection was not specific to cancer cells; HSV1 or VSVΔ51 infection also exhibited enhanced spread following shRNA-mediated knockdown of *Inpp5e* in the normal fibroblast cell line NIH 3T3 (Figures S6F and S6G). The response in NIH 3T3 was more attenuated than that in 4T1 $Inpp5e^{CRISPR}$ cells at 48 h post-infection (compare Figures 6C

(E) Top: schematic of the cold-binding assays. $Inpp5e^{CRISPR}$ and $Inpp5e^{+/+}$ cells were incubated at 4°C with HSV1 at an MOI of 10 for 1 h (attachment assay) or 4°C for 1 h followed by 37°C for 1 h (internalization assay). Total DNA was extracted and viral UL30 DNA was quantified by qPCR and normalized to cellular *Lmnb2* DNA. Bottom: graphs presenting the effect of $Inpp5e^{CRISPR}$ on virus attachment (left), internalization (center), and the contribution of internalization versus attachment in each cell type expressed as a ratio (right).

(F) HSV1-K26-GFP cold-binding assay. As in (E), but using a virus decorated with a GFP-fusion coat protein that allowed the detection of diffraction-limited puncta by confocal microscopy in fixed cells. Images are single confocal slices representing the mid-cell region. Nuclei are stained with Hoechst. DIC, differential interference contrast.

Error bars indicate standard error of the mean (sem). *p<0.05, **p<0.01, ***p<0.001, ns, non-significant, calculated using two-tailed *t*-test.

and S6F). However, we cannot rule out the possibility that this was due to residual INPP5E present in the NIH 3T3 cells. As a proxy measurement for viral binding and/or entry, we modified the classical plaque assay by infecting a monolayer of live or *Inpp5e*$^{+/+}$ 4T1 cells in an agar matrix (to prevent cell-to-cell spread of virion) with HSV1, VSVΔ51, or VACV at very low MOI (0.01). *Inpp5e*$^{CRISPR}$ cells generated >2-fold more plaques when exposed to HSV1 in contrast to no change in the number of VACV or VSVΔ51 plaques (Figure 6D). These data suggest that viral binding and/or entry of HSV1 is enhanced in *Inpp5e*$^{CRISPR}$ cells.

To further investigate the role of INPP5E in early HSV1 infection, we separately assessed cell attachment or internalization of virions using two parallel cold-binding assays (Figure 6E, schema at top) that quantified virus particles via qPCR of HSV1 genomic DNA (gDNA) copies (Mar et al., 2018). In the attachment assay, 6.8- and 4.3-fold more viral DNA was found to be associated with the surface-bound fraction in *Inpp5e*$^{CRISPR\#1}$ and *Inpp5e*$^{CRISPR\#2}$ versus *Inpp5e*$^{+/+}$ cells, respectively (Figure 6E, lower left). A similar trend was measured with the internalization assay, in which 4.4- and 6.4-fold more viral DNA was found within *Inpp5e*$^{CRISPR\#1}$ and *Inpp5e*$^{CRISPR\#2}$ cells, respectively, relative to control cells (Figure 6E, lower center). The internalization:attachment ratio did not significantly change in the *Inpp5e*$^{CRISPR}$ cells, indicating that the binding of HSV1 virions to the cell surface is significantly enhanced independently of internalization (Figure 6E, lower right). Furthermore, in a parallel cold-binding experiment using HSV1 expressing a GFP fusion of the capsid protein VP26, which allows visualization of virions as diffraction-limited puncta, a sizable increase in the number of GFP puncta binding to *Inpp5e*$^{CRISPR}$ cells was observed (Figure 6F).

These data define translationally regulated antiviral effectors, with the phosphatidylinositol (PI) phosphatase INPP5E being further characterized in our study. While INPP5E is translationally induced by all three of the viruses we assayed, its expression appears to have a pronounced antiviral effect in the context of HSV1 infection, modulating viral attachment to and spread between host cells.

## DISCUSSION

To thwart virus infection, mammalian cells suppress the activity of their mRNA translation machinery, while viruses often attempt to take control of it to maximize translation of their own mRNAs (Hoang et al., 2018; Walsh et al., 2013). However, the synthesis of antiviral proteins is still needed, and single-gene studies have shown that some of these transcripts are uniquely upregulated at the translation level, distinct from transcriptionally induced ISGs (Colina et al., 2008; Herdy et al., 2012). Our present work reveals a global profile of host cellular mRNAs differentially translated in a breast cancer cell model infected by clinically relevant oncolytic viruses.

We find that translationally regulated mRNAs in this context are functionally enriched in proteins involved in primary cilium homeostasis. Our sentinel gene, *INPP5E*, is a target of genetic mutation in humans, responsible for ciliopathies such as Joubert syndrome and mental retardation, truncal obesity, retinal dystrophy, and micropenis (MORM) syndrome (Jacoby et al., 2009). Mainly localized at the primary cilium, it has also been observed within the nucleus and at centrioles (Sierra Potchanant et al., 2017). Our IF data in poly(I:C)- or VACV-treated cells shows a punctate distribution pattern of induced INPP5E that is reminiscent of vesicles. This is perhaps unsurprising, given the presumed membrane localization of INPP5E, with its C-terminal farnesylation and its role in modifying PI signaling (Jacoby et al., 2009). INPP5E is an inositol 5-polyphosphatase, and therefore likely controls second messenger PI signaling at vesicular structures as it does within the cilium, where it maintains a high concentration of PI-4-phosphate (PI(4)P) relative to PI(4,5)$P_2$, an attribute linked to ciliary stability (Dyson et al., 2017; Phua et al., 2017). Another second messenger, PI(5)P, is induced by Newcastle disease virus infection and poly(I:C) and can act as an innate immune effector promoting type I IFN production through the TANK-binding kinase 1 (TBK1)-IRF3 signaling axis (Kawasaki et al., 2013). Several viruses activate PI3K signaling pathways (Walsh et al., 2013); this increases PI(3,4,5)$P_3$ and consequently activates the Akt-mTOR signaling axis, thus modulating infection efficiency. PI(4,5)$P_2$ and PI(3,4,5)$P_3$, two likely INPP5E substrates, are well-known mediators of actin remodeling (Saarikangas et al., 2010). We found a positive effect of INPP5E removal on both HSV1 and VSVΔ51 infections, and this may be explained by changes to the actin cytoskeleton (e.g., changes in membrane ruffling that alter viral attachment) (Taylor et al., 2011). Consistent with this hypothesis, we observed enhanced binding of HSV1 to the cell surface, while internalization remained unaffected. While INPP5E can be localized to the cilium, viral attachment did not appear to be polarized as one would expect if enhanced binding occurred at or near ciliary structures. Thus, INPP5E antiviral activities may be not related to its ciliary localization. Away from the plasma membrane, centrosomal PIs can also be affected by a lack of INPP5E, leading to spindle microtubule destabilization, possibly through an imbalance in PI(4,5)$P_2$ expression (Sierra Potchanant et al., 2017). Whether these mechanisms have a role to play in mediating the enhanced virus binding and infection seen in 4T1 cells is subject to future investigation.

Another ciliary gene we examined, *BBS9*, encodes a protein that serves as a structural component of the BBSome, a stoichiometric, octameric protein complex (composed of BBS1, -2, -5, -7, -8, -9, and -10) charged with receptor cargo destined for the primary cilium (Nachury et al., 2007); however, others have shown that the BBSome is important in the transport of extra-ciliary cargo to the plasma membrane (Starks et al., 2015) and in retrograde transport (Yen et al., 2006). Mutations in *BBS9* and other *BBS* genes underlie Bardet-Biedel syndrome, a rare pleiotropic disorder that is thought to arise from cilia dysfunction. We have found that akin to INPP5E, BBS9 expression limits HSV1, VACV, and VSVΔ51 infections. Whether impaired BBSome function is responsible for the proviral effect that we observed with BBS9 knockdown in 4T1 cells will require more investigation. BBS9 might instead display BBSome-independent antiviral functions.

We show here that translationally upregulated mRNAs common to all three infections were normally repressed at the level of translation in the uninfected condition. In a search for a mechanistic explanation of this repression-de-repression switch, we

noted an enrichment of uORFs in their 5′ leaders, a *cis*-acting sequence element that can confer translational de-repression during the accumulation of P-eIF2α (Barbosa et al., 2013). Further investigation using *Inpp5e* 5′ leader reporter assays revealed no uORF-dependent de-repression during infection. Instead, a variant switch during infection with HSV1 or VACV or upon treatment with the viral mimic poly(I:C) was observed, producing an alternatively transcribed and spliced transcript with a shortened *Inpp5e* 5′ leader. Critically, we found that the spliced 5′ leader intron harbors repressive uORFs, and consequently, the short *Inpp5e* 5′ leader is a better substrate for translation than its longer, unspliced counterpart. We also found enrichment of binding motifs for the splicing factors SRSF1 and SRSF9 in the 5′ leader of translationally regulated genes, again, suggestive of a role for alternative splicing in modifying translation of these genes. Thus, our study presents evidence for a regulatory mechanism in which translational output of an antiviral gene is modulated via a transcript variant shift that increases expression of a normally minor variant that harbors a less translationally repressive leader.

These findings are in line with previous studies proposing a role for regulating protein synthesis via transcript variants (Floor and Doudna, 2016) and follows the axiom that alternative transcription and splicing increases transcriptome diversity from a more limited and inflexible genome. Clearly, differences in the coding region between transcript variants can produce functionally different protein isoforms, but differences in the non-coding regions (5′ leader and 3′ UTR) similarly confer important changes to protein function by altering protein abundance in time and space (Floor and Doudna, 2016; Mayr and Bartel, 2009). These regions contain *cis*-elements that regulate mRNA turnover, location, and/or translation. They can be altered via alternative transcription, splicing, start-site selection, or alternative polyadenylation and termination. Examples of differential transcript variant expression have been reported during infection with various viruses (Ku et al., 2011; Wang et al., 2018). More specifically, RNA sequencing (RNA-seq) has revealed widespread disturbances to host transcription termination caused by HSV1 infection (Rutkowski et al., 2015) and has identified HSV1 ICP27 protein as a major viral factor responsible for modulating the host transcript variant landscape (Tang et al., 2016). Aberrant splicing can lead to defective innate immunity during the host response to virus infection. For instance, the lack of the RNA-binding protein BUD13 causes the retention of the 4$^{th}$ intron in human *IRF7* upon stimulation by poly(I:C) or IFN-α, generating a defective mRNA and impaired antiviral response when challenged with VSV (Frankiw et al., 2019). In the present study, we observed the opposite effect from both a mechanistic and a phenotypic perspective: viral infection or poly(I:C) treatment caused splicing of an intron and potentiation of the host antiviral response, rather than intron retention and abrogation of that response. The question remains: How does infection signal the switch to an alternative "ribosome-engaged" transcriptome? PKR-mediated splicing has been previously reported (Ilan et al., 2017); however, we were unable to link PKR activation to our change in variant expression. Further studies will be required to home in on the signaling axis that mediates the increased expression of the short *Inpp5e* transcript.

In summary, we describe herein a post-transcriptional mechanism for the appropriate expression of potent antiviral genes. Our data suggest that innate immunity projects a complicated regulatory landscape in which various host and viral factors are translationally modulated through interactions with pre-mRNA and splicing complexes. In cataloging the genes that are part of the translational arm of innate immunity, we have uncovered regulatory nodes that may benefit from future study with the goal of improving cancer therapeutics.

## STAR★METHODS

Detailed methods are provided in the online version of this paper and include the following:

- KEY RESOURCES TABLE
- LEAD CONTACT AND MATERIALS AVAILABILITY
- EXPERIMENTAL MODEL AND SUBJECT DETAILS
  - Cell culture and viruses
- METHOD DETAILS
  - Lentivirus production and plasmids
  - Poly(I:C) treatment
  - Polysome profiling
  - Metabolic labeling and cell viability
  - Ribosome profiling
  - Mapping and analysis of ribosome profiling data
  - Functional analysis of DEGs
  - Immunocytochemistry
  - Western blotting
  - Quantitative RT-PCR (RT-qPCR) and Droplet Digital RT-PCR (RT-ddPCR)
  - CAT translation reporter assays
  - CRISPR/Cas9-mediated gene knockout
  - Live cell monitoring of virus spread
  - Plaque assays
  - Binding assays
- QUANTIFICATION AND STATISTICAL ANALYSES
- DATA AND CODE AVAILABILITY

### SUPPLEMENTAL INFORMATION

Supplemental Information can be found online at https://doi.org/10.1016/j.celrep.2019.11.072.

### ACKNOWLEDGMENTS

We thank Drs. John Bell, Martin Holcik, Antonis Koromilas, Karen Mossman and David Stojdl for materials used in the experiments. H.-D.H. is a recipient of a University of Ottawa Graduate Scholarship, an Ontario Graduate Scholarship, and a University of Ottawa Faculty of Medicine Destination 2020 Scholarship. This work was supported in part by the Canadian Breast Cancer Foundation/Canadian Cancer Society Research Institute, the Cancer Research Society/CIHR Institute of Cancer Research (grant 22124), the Natural Sciences and Engineering Research Council of Canada (RGPIW-2016-05228), and the Terry Fox Research Institute (New Frontier Program Project Grant, to T.A. and T.E.G.).

### AUTHOR CONTRIBUTIONS

T.A., H.-D.H., T.E.G., and S.M.J. conceived and designed the experiments. H.-D.H. and T.E.G. performed the majority of the experiments, including the

functional analysis of the ribosome-profiling data. H.-D.H., T.E.G., and T.A. wrote the manuscript. J.-J.J. produced the viruses and performed the viral titer assays. N.V. performed the heterologous reporter assays. V.H.G. performed the western blotting. X.X. performed qRT-PCR. T.A., C.G.G., and S.M.J. performed the wet component of the ribosome profiling. W.L. performed the ribosome-profiling mapping. K.N.C., M.J., and T.A. reviewed and edited the final manuscript. All of the authors read and approved the final manuscript.

## DECLARATION OF INTERESTS

The authors declare no competing interests.

Received: July 2, 2019
Revised: October 16, 2019
Accepted: November 15, 2019
Published: December 17, 2019

## REFERENCES

Abernathy, E., Clyde, K., Yeasmin, R., Krug, L.T., Burlingame, A., Coscoy, L., and Glaunsinger, B. (2014). Gammaherpesviral gene expression and virion composition are broadly controlled by accelerated mRNA degradation. PLoS Pathog. *10*, e1003882.

Barbosa, C., Peixeiro, I., and Romão, L. (2013). Gene expression regulation by upstream open reading frames and human disease. PLoS Genet. *9*, e1003529.

Blais, J.D., Filipenko, V., Bi, M., Harding, H.P., Ron, D., Koumenis, C., Wouters, B.G., and Bell, J.C. (2004). Activating transcription factor 4 is translationally regulated by hypoxic stress. Mol. Cell. Biol. *24*, 7469–7482.

Boldt, K., van Reeuwijk, J., Lu, Q., Koutroumpas, K., Nguyen, T.M., Texier, Y., van Beersum, S.E., Horn, N., Willer, J.R., Mans, D.A., et al.; UK10K Rare Diseases Group (2016). An organelle-specific protein landscape identifies novel diseases and molecular mechanisms. Nat. Commun. *7*, 11491.

Brinkman, E.K., Chen, T., Amendola, M., and van Steensel, B. (2014). Easy quantitative assessment of genome editing by sequence trace decomposition. Nucleic Acids Res. *42*, e168.

Colina, R., Costa-Mattioli, M., Dowling, R.J.O., Jaramillo, M., Tai, L.-H., Breitbach, C.J., Martineau, Y., Larsson, O., Rong, L., Svitkin, Y.V., et al. (2008). Translational control of the innate immune response through IRF-7. Nature *452*, 323–328.

Dai, A., Cao, S., Dhungel, P., Luan, Y., Liu, Y., Xie, Z., and Yang, Z. (2017). Ribosome Profiling Reveals Translational Upregulation of Cellular Oxidative Phosphorylation mRNAs during Vaccinia Virus-Induced Host Shutoff. J. Virol. *91*, e01858-e16.

Desai, P., and Person, S. (1998). Incorporation of the green fluorescent protein into the herpes simplex virus type 1 capsid. J. Virol. *72*, 7563–7568.

Diallo, J.-S., Vähä-Koskela, M., Le Boeuf, F., and Bell, J. (2012). Propagation, Purification, and In Vivo Testing of Oncolytic Vesicular Stomatitis Virus Strains. Methods Mol. Biol. *797*, 127–140.

Dyson, J.M., Conduit, S.E., Feeney, S.J., Hakim, S., DiTommaso, T., Fulcher, A.J., Sriratana, A., Ramm, G., Horan, K.A., Gurung, R., et al. (2017). INPP5E regulates phosphoinositide-dependent cilia transition zone function. J. Cell Biol. *216*, 247–263.

Fields, A.P., Rodriguez, E.H., Jovanovic, M., Stern-Ginossar, N., Haas, B.J., Mertins, P., Raychowdhury, R., Hacohen, N., Carr, S.A., Ingolia, N.T., et al. (2015). A Regression-Based Analysis of Ribosome-Profiling Data Reveals a Conserved Complexity to Mammalian Translation. Mol. Cell *60*, 816–827.

Floor, S.N., and Doudna, J.A. (2016). Tunable protein synthesis by transcript isoforms in human cells. eLife *5*, e10921.

Frankiw, L., Majumdar, D., Burns, C., Vlach, L., Moradian, A., Sweredoski, M.J., and Baltimore, D. (2019). BUD13 Promotes a Type I Interferon Response by Countering Intron Retention in Irf7. Mol. Cell *73*, 803–814.e6.

Gandin, V., Sikström, K., Alain, T., Morita, M., McLaughlan, S., Larsson, O., and Topisirovic, I. (2014). Polysome fractionation and analysis of mammalian translatomes on a genome-wide scale. J. Vis. Exp. (*87*) https://doi.org/10.3791/51455.

Gordon, A. (2010). FASTX-Toolkit. FASTQ/A short-reads pre-processing tools. http://hannonlab.cshl.edu/fastx_toolkit/.

Graber, T.E., Baird, S.D., Kao, P.N., Mathews, M.B., and Holcik, M. (2010). NF45 functions as an IRES trans-acting factor that is required for translation of cIAP1 during the unfolded protein response. Cell Death Differ. *17*, 719–729.

Harrington, K., Freeman, D.J., Kelly, B., Harper, J., and Soria, J.-C. (2019). Optimizing oncolytic virotherapy in cancer treatment. Nat. Rev. Drug Discov. *18*, 689–706.

Herdy, B., Jaramillo, M., Svitkin, Y.V., Rosenfeld, A.B., Kobayashi, M., Walsh, D., Alain, T., Sean, P., Robichaud, N., Topisirovic, I., et al. (2012). Translational control of the activation of transcription factor NF-κB and production of type I interferon by phosphorylation of the translation factor eIF4E. Nat. Immunol. *13*, 543–550.

Hoang, H.-D., Graber, T.E., and Alain, T. (2018). Battling for Ribosomes: Translational Control at the Forefront of the Antiviral Response. J. Mol. Biol. *430*, 1965–1992.

Ilan, L., Osman, F., Namer, L.S., Eliahu, E., Cohen-Chalamish, S., Ben-Asouli, Y., Banai, Y., and Kaempfer, R. (2017). PKR activation and eIF2α phosphorylation mediate human globin mRNA splicing at spliceosome assembly. Cell Res. *27*, 688–704.

Ingolia, N.T., Ghaemmaghami, S., Newman, J.R.S., and Weissman, J.S. (2009). Genome-wide analysis in vivo of translation with nucleotide resolution using ribosome profiling. Science *324*, 218–223.

Jacoby, M., Cox, J.J., Gayral, S., Hampshire, D.J., Ayub, M., Blockmans, M., Pernot, E., Kisseleva, M.V., Compère, P., Schiffmann, S.N., et al. (2009). INPP5E mutations cause primary cilium signaling defects, ciliary instability and ciliopathies in human and mouse. Nat. Genet. *41*, 1027–1031.

Jafarnejad, S.M., Chapat, C., Matta-Camacho, E., Gelbart, I.A., Hesketh, G.G., Arguello, M., Garzia, A., Kim, S.-H., Attig, J., Shapiro, M., et al. (2018). Translational control of ERK signaling through miRNA/4EHP-directed silencing. eLife *7*, e35034.

Johansson, P.J., Myhre, E.B., and Blomberg, J. (1985). Specificity of Fc receptors induced by herpes simplex virus type 1: comparison of immunoglobulin G from different animal species. J. Virol. *56*, 489–494.

Katz, Y., Wang, E.T., Airoldi, E.M., and Burge, C.B. (2010). Analysis and design of RNA sequencing experiments for identifying isoform regulation. Nat. Methods *7*, 1009–1015.

Kawasaki, T., Takemura, N., Standley, D.M., Akira, S., and Kawai, T. (2013). The second messenger phosphatidylinositol-5-phosphate facilitates antiviral innate immune signaling. Cell Host Microbe *14*, 148–158.

Ku, C.-C., Che, X.-B., Reichelt, M., Rajamani, J., Schaap-Nutt, A., Huang, K.-J., Sommer, M.H., Chen, Y.-S., Chen, Y.-Y., and Arvin, A.M. (2011). Herpes simplex virus-1 induces expression of a novel MxA isoform that enhances viral replication. Immunol. Cell Biol. *89*, 173–182.

Langmead, B., and Salzberg, S.L. (2012). Fast gapped-read alignment with Bowtie 2. Nat. Methods *9*, 357–359.

Lee, S., Liu, B., Lee, S., Huang, S.X., Shen, B., and Qian, S.B. (2012). Global mapping of translation initiation sites in mammalian cells at single-nucleotide resolution. Proc. Natl. Acad. Sci. USA *109*, E2424–E2432.

Leppek, K., Das, R., and Barna, M. (2018). Functional 5′ UTR mRNA structures in eukaryotic translation regulation and how to find them. Nat. Rev. Mol. Cell Biol. *19*, 158–174.

Maere, S., Heymans, K., and Kuiper, M. (2005). BiNGO: a Cytoscape plugin to assess overrepresentation of gene ontology categories in biological networks. Bioinformatics *21*, 3448–3449.

Mar, K.B., Rinkenberger, N.R., Boys, I.N., Eitson, J.L., McDougal, M.B., Richardson, R.B., and Schoggins, J.W. (2018). LY6E mediates an evolutionarily conserved enhancement of virus infection by targeting a late entry step. Nat. Commun. *9*, 3603.

Mayr, C., and Bartel, D.P. (2009). Widespread shortening of 3′UTRs by alternative cleavage and polyadenylation activates oncogenes in cancer cells. Cell *138*, 673–684.

Nachury, M.V., Loktev, A.V., Zhang, Q., Westlake, C.J., Peränen, J., Merdes, A., Slusarski, D.C., Scheller, R.H., Bazan, J.F., Sheffield, V.C., and Jackson, P.K. (2007). A core complex of BBS proteins cooperates with the GTPase Rab8 to promote ciliary membrane biogenesis. Cell *129*, 1201–1213.

Oliveros, J.C. (2007). VENNY. An interactive tool for comparing lists with Venn Diagrams. https://bioinfogp.cnb.csic.es/tools/venny/index.html.

Phua, S.C., Chiba, S., Suzuki, M., Su, E., Roberson, E.C., Pusapati, G.V., Setou, M., Rohatgi, R., Reiter, J.F., Ikegami, K., and Inoue, T. (2017). Dynamic Remodeling of Membrane Composition Drives Cell Cycle through Primary Cilia Excision. Cell *168*, 264–279.e15.

Riley, A., Jordan, L.E., and Holcik, M. (2010). Distinct 5′ UTRs regulate XIAP expression under normal growth conditions and during cellular stress. Nucleic Acids Res. *38*, 4665–4674.

Rutkowski, A.J., Erhard, F., L'Hernault, A., Bonfert, T., Schilhabel, M., Crump, C., Rosenstiel, P., Efstathiou, S., Zimmer, R., Friedel, C.C., and Dölken, L. (2015). Widespread disruption of host transcription termination in HSV-1 infection. Nat. Commun. *6*, 7126.

Saarikangas, J., Zhao, H., and Lappalainen, P. (2010). Regulation of the actin cytoskeleton-plasma membrane interplay by phosphoinositides. Physiol. Rev. *90*, 259–289.

Sanjana, N.E., Shalem, O., and Zhang, F. (2014). Improved vectors and genome-wide libraries for CRISPR screening. Nat. Methods *11*, 783–784.

Schneider, W.M., Chevillotte, M.D., and Rice, C.M. (2014). Interferon-stimulated genes: a complex web of host defenses. Annu. Rev. Immunol. *32*, 513–545.

Schoggins, J.W., Wilson, S.J., Panis, M., Murphy, M.Y., Jones, C.T., Bieniasz, P., and Rice, C.M. (2011). A diverse range of gene products are effectors of the type I interferon antiviral response. Nature *472*, 481–485.

Schwanhäusser, B., Busse, D., Li, N., Dittmar, G., Schuchhardt, J., Wolf, J., Chen, W., and Selbach, M. (2011). Global quantification of mammalian gene expression control. Nature *473*, 337–342.

Sendoel, A., Dunn, J.G., Rodriguez, E.H., Naik, S., Gomez, N.C., Hurwitz, B., Levorse, J., Dill, B.D., Schramek, D., Molina, H., et al. (2017). Translation from unconventional 5′ start sites drives tumour initiation. Nature *541*, 494–499.

Shannon, P., Markiel, A., Ozier, O., Baliga, N.S., Wang, J.T., Ramage, D., Amin, N., Schwikowski, B., and Ideker, T. (2003). Cytoscape: a software environment for integrated models of biomolecular interaction networks. Genome Res. *13*, 2498–2504.

Shi, Z., and Barna, M. (2015). Translating the genome in time and space: specialized ribosomes, RNA regulons, and RNA-binding proteins. Annu. Rev. Cell Dev. Biol. *31*, 31–54.

Sierra Potchanant, E.A., Cerabona, D., Sater, Z.A., He, Y., Sun, Z., Gehlhausen, J., and Nalepa, G. (2017). INPP5E Preserves Genomic Stability through Regulation of Mitosis. Mol. Cell. Biol. *37*, e00500-16.

Sonenberg, N., and Hinnebusch, A.G. (2009). Regulation of translation initiation in eukaryotes: mechanisms and biological targets. Cell *136*, 731–745.

Starks, R.D., Beyer, A.M., Guo, D.F., Boland, L., Zhang, Q., Sheffield, V.C., and Rahmouni, K. (2015). Regulation of Insulin Receptor Trafficking by Bardet Biedl Syndrome Proteins. PLoS Genet. *11*, e1005311.

Stojdl, D.F., Lichty, B.D., TenOever, B.R., Paterson, J.M., Power, A.T., Knowles, S., Marius, R., Reynard, J., Poliquin, L., Atkins, H., et al. (2003). VSV strains with defects in their ability to shutdown innate immunity are potent systemic anti-cancer agents. Cancer Cell *4*, 263–275.

Tang, S., Patel, A., and Krause, P.R. (2016). Herpes simplex virus ICP27 regulates alternative pre-mRNA polyadenylation and splicing in a sequence-dependent manner. Proc. Natl. Acad. Sci. USA *113*, 12256–12261.

Taylor, M.P., Koyuncu, O.O., and Enquist, L.W. (2011). Subversion of the actin cytoskeleton during viral infection. Nat. Rev. Microbiol. *9*, 427–439.

Tebaldi, T., Re, A., Viero, G., Pegoretti, I., Passerini, A., Blanzieri, E., and Quattrone, A. (2012). Widespread uncoupling between transcriptome and translatome variations after a stimulus in mammalian cells. BMC Genomics *13*, 220.

Tirosh, O., Cohen, Y., Shitrit, A., Shani, O., Le-Trilling, V.T.K., Trilling, M., Friedlander, G., Tanenbaum, M., and Stern-Ginossar, N. (2015). The Transcription and Translation Landscapes during Human Cytomegalovirus Infection Reveal Novel Host-Pathogen Interactions. PLoS Pathog. *11*, e1005288.

Walsh, D., Mathews, M.B., and Mohr, I. (2013). Tinkering with translation: protein synthesis in virus-infected cells. Cold Spring Harb. Perspect. Biol. *5*, a012351.

Wang, X., Hou, J., Quedenau, C., and Chen, W. (2016). Pervasive isoform-specific translational regulation via alternative transcription start sites in mammals. Mol. Syst. Biol. *12*, 875.

Wang, P.-H., Fung, S.-Y., Gao, W.-W., Deng, J.-J., Cheng, Y., Chaudhary, V., Yuen, K.-S., Ho, T.-H., Chan, C.-P., Zhang, Y., et al. (2018). A novel transcript isoform of STING that sequesters cGAMP and dominantly inhibits innate nucleic acid sensing. Nucleic Acids Res. *46*, 4054–4071.

Yen, H.-J., Tayeh, M.K., Mullins, R.F., Stone, E.M., Sheffield, V.C., and Slusarski, D.C. (2006). Bardet-Biedl syndrome genes are important in retrograde intracellular trafficking and Kupffer's vesicle cilia function. Hum. Mol. Genet. *15*, 667–677.

Zakaria, C., Sean, P., Hoang, H.-D., Leroux, L.-P., Watson, M., Workenhe, S.T., Hearnden, J., Pearl, D., Truong, V.T., Robichaud, N., et al. (2018). Active-site mTOR inhibitors augment HSV1-dICP0 infection in cancer cells via dysregulated eIF4E/4E-BP axis. PLoS Pathog. *14*, e1007264.

## STAR★METHODS

### KEY RESOURCES TABLE

| REAGENT or RESOURCE | SOURCE | IDENTIFIER |
|---|---|---|
| Antibodies | | |
| Mouse anti-INPP5E | Abcam | ab69696, RRID:AB_2126254 |
| Rabbit anti-INPP5E | Cohesion Biosciences | CPA3073 |
| Mouse anti- β-actin | Sigma | A5441, AB_476744 |
| Mouse anti-GAPDH | Abcam | Ab8245, RRID:AB_2107448 |
| Rabbit anti-HSV1 | Dako | B011402 |
| Mouse anti-HSV1 ICP0 | Santa Cruz | 11060, RRID:AB_673704 |
| Bacterial and Virus Strains | | |
| HSV1 (HSV1716, strain 17 – g34.5 deleted) | Sorrento Therapeutic, San Diego, US | N/A |
| VACV (Jennerex-594, strain Wyeth, Tk-deleted expressing GM-CSF) | Sillagen, Seoul, Republic of Korea | N/A |
| Reovirus (Reolysin, Type 3 Dearing) | Oncolytics Biotech, Calgary, Canada | N/A |
| VSVΔ51-RFP (ΔM51 with insertion of RFP marker | Stojdl et al., 2003 | N/A |
| HSV1-K26-GFP (HSV1 with insertion of GFP to vp26) | Desai and Person, 1998 | N/A |
| Biological Samples | | |
| DMEM | Fisher | SH30022FS |
| RPMI | Fisher | SH30027FS |
| FBS | Sigma | F1051 |
| Penicillin/Streptomycin | Fisher | sv30010 |
| Chemicals, Peptides, and Recombinant Proteins | | |
| High Molecular Weight poly(I:C) | InvivoGen | tlrl-pic |
| Lipofectamine 2000 | Fisher | 11668019 |
| EasyTagTM Express Protein Labeling Mix | Perkin Elmer | NEG772002MC |
| Critical Commercial Assays | | |
| Cell Proliferation Kit I – MTT | Roche | 11465007001 |
| CAT ELISA | Roche | 11363727001 |
| Deposited Data | | |
| Ribosome footprint of infected cancer cells | This study | GEO: GSE137757 |
| RNaseq of transcriptome of infected cancer cells | This study | GEO: GSE137757 |
| Experimental Models: Cell Lines | | |
| 4T1 | ATCC | CRL-2539, RRID:CVCL_0125 |
| HEK293T | ATCC | CRL-3216, CVCL_0063 |
| CT-2A | Laboratory of D. Stojdl | N/A |
| PKR-null/WT MEFs | Laboratory of A. Koromilas | N/A |
| NIH 3T3 | ATCC | CRL-1658, CVCL_0594 |
| Oligonucleotides | | |
| See Table S4 | N/A | N/A |
| Recombinant DNA | | |
| shNTC plasmid DNA (MISSION® pLKO.1-puro Non-Mammalian shRNA Control Plasmid DNA) | Sigma | SHC002 |
| shINPP5E plasmid DNA (MISSION® shRNA plasmid DNA) | Sigma | TRCN0000080705 |

(*Continued on next page*)

*Continued*

| REAGENT or RESOURCE | SOURCE | IDENTIFIER |
|---|---|---|
| shBBS9 plasmid DNA (MISSION® shRNA plasmid DNA) | Sigma | TRCN0000182387 |
| shUSP18 plasmid DNA (MISSION® shRNA plasmid DNA) | Sigma | TRCN0000030789 |
| shUSP44 plasmid DNA (MISSION® shRNA plasmid DNA) | Sigma | TRCN0000030879 |
| Software and Algorithms | | |
| FASTX | Laboratory of G. Hannon | http://hannonlab.cshl.edu/fastx_toolkit/ |
| Bowtie2 | Langmead and Salzberg, 2012 | http://bowtie-bio.sourceforge.net/bowtie2/index.shtml |
| Venny v2.1 | Oliveros, 2007 | https://bioinfogp.cnb.csic.es/tools/venny_old/venny.php |
| BiNGO | Maere et al., 2005 | http://apps.cytoscape.org/apps/bingo |
| Cytoscape 3.0 | Shannon et al., 2003 | https://www.cytoscape.org |

## LEAD CONTACT AND MATERIALS AVAILABILITY

Further information and request for resources and reagents should be directed to and will be fulfilled by the Lead Contact, Dr. Tommy Alain (tommy@mgcheo3.med.uottawa.ca). Material will be made available upon reasonable request.

## EXPERIMENTAL MODEL AND SUBJECT DETAILS

### Cell culture and viruses

Mouse breast carcinoma 4T1, fibroblast NIH 3T3, human HEK293T and monkey Vero cells were obtained from American Type Culture Collection (ATCC). Mouse glioblastoma CT2A was obtained from Dr. David Stojdl (Children's Hospital of Eastern Ontario Research Institute). PKR null and respective wild-type MEFs were obtained from Dr. Antonis Koromilas (Lady Davis Institute). Cells were routinely checked for mycoplasma contamination by cytoplasmic DNA staining. NIH 3T3, HEK293T, Vero, CT2A and MEFs were cultured in Dulbecco's Modified Eagle Medium (DMEM) (Fisher) supplemented with 10% fetal bovine serum (Sigma) and 0.1% penicillin and streptomycin (Life Technologies) at 37°C in 5% $CO_2$. 4T1 were cultured in Roswell Park Memorial Institute (RPMI) 1640 (Fisher) supplemented with 10% fetal bovine serum (Wisent Bioproducts) and 0.1% penicillin and streptomycin. HSV1 (HSV1-1716, strain 17 – γ34.5 deleted, Sorrento Therapeutics, San Diego, USA), VACV (JX-594 strain Wyeth, Tk-deleted expressing GM-CSF, Jennerex Biotherapeutics / Sillagen, Seoul, Republic of Korea) and Reovirus (Reolysin, Type 3 Dearing, – Oncolytics Biotech, Calgary, Canada) were kindly provided by manufacturers. VSVΔ51-RFP (ΔM51 with insertion of RFP marker) was kindly provided by Dr. John Bell (Ottawa Hospital Research Institute). HSV1-K26-GFP was kindly provided by Dr. Karen Mossman (McMaster University). For propagation of HSV1-1716 and HSV1-K26-GFP, monolayer of Vero cells was inoculated with viruses at a MOI of 0.5 and cultured for 72 hours at 37°C, 5% $CO_2$. Supernatant was clarified by centrifuge at 500 x g for 5 min, then filtered (0.45 μm). Virus particles in the supernatant were separated from cellular debris by ultracentrifugation at 17500 x g for 90 min over a sucrose cushion (36% sucrose, 10 mM HEPES, 150 mM NaCl, 0.1 mM EDTA, pH 7.3). Pellets were resuspended in 1X HNE buffer (10 mM HEPES, 150 mM NaCl, 0.1 mM EDTA, pH 7.3) and stored at −80°C. VSVΔ51 propagation was adapted from a previously described method (Diallo et al., 2012). Briefly, monolayer of Vero cells was inoculated with VSVΔ51 at MOI of 0.01. Approximately 24 hours post inoculation, supernatant was collected and clarified by centrifugation at 500 x g for 5 min. Cleared supernatant are filtered (0.2 μm), then virus particles were pelleted by ultracentrifugation at 28,000 x g for 90 min. Virus particles in the pellet were resuspended in DMEM media and stored at −80°C. JX-594 and Reovirus were used directly from stock provided by manufacturer.

## METHOD DETAILS

### Lentivirus production and plasmids

The following lentiviral vectors were obtained from Sigma Aldrich: SHC002 (shNTC); TRCN0000080705 (shINPP5E); TRCN0000182387 (shBBS9), TRCN0000030789 (shUSP18), TRCN0000030879 (shUSP44). The lentiviral vectors were co-transfected with the packaging plasmids pLP1, pLP2 and pLP/VSVG (Thermofisher) into HEK293T cells. Lentivirus-containing supernatants were collected at 48 and 72 hours post-transfection and filtered (0.45 μm). The filtrate was applied directly to target cells and integration of the expression cassette was confirmed 72 hours post-transduction by puromycin selection at 2 μg/ml for 4 days. The long mouse *Inpp5e* 5′ leader (nt 1-601) was PCR-amplified from a full-length MGC cDNA clone (GenBank: BC052717; cloneID 6837339 from Dharmacon). This clone is missing the first 31 nucleotides of the annotated long *Inpp5e* mRNA transcript

(NM_033134). The 601 nt 5′ leader was cloned into the NotI restriction site of pMC (a kind gift of Dr. Martin Holcik, Carleton University) upstream of the CAT reporter maintaining the same reading frame as the endogenouse *Inpp5e* transcript. The short *Inpp5e* leader (found in NM_001290437; nt 1-348) was created from the long-leader CAT construct by a deletion overlap extension cloning strategy. Site-directed mutagenesis was performed to mutate uORF start codons in the long-leader CAT construct. All constructs were verified by Sanger sequencing.

### Poly(I:C) treatment

Cells was transfecting with high molecular weight poly(I:C) (InvivoGen) using Lipofectamine 2000 (Thermo Fisher) according to the manufacturer protocol at a ratio of 1:2 μg:μl poly(I:C):lipofectamine. A poly(I:C) concentration of 5 μg/ml was used unless otherwise indicated. For "vehicle" treatments, cells were transfected with lipofectamine 2000 but without poly(I:C).

### Polysome profiling

Polysome profiling was conducted as previously described (Gandin et al., 2014). Briefly, cycloheximide (Bioshop, CAT #66-81-9) was added directly to the culture media to a final concentration of 100 μg/ml and incubated for 5 min. Cells were then washed 3 times with ice cold PBS containing cycloheximide, then were scraped from the dishes and pelleted at 500 x g for 5 min at 4°C. Cells were lysed with hypotonic buffer (5 mM Tris pH 7.5, 2.5 mM $MgCl_2$, 1.5 mM KCl) supplemented with cOmplete Protease Inhibitor Cocktail (Roche) and debris was cleared by centrifugation at 14,000 x g for 5 min, 4°C. Lysates containing ribosome-bound mRNAs were collected, flash frozen, then stored at −80°C. A volume of lysate equal to 10 OD260 units was added on a 10%–50% sucrose gradient and centrifuged at 36,000 rpm in a SW41 bucket rotor for 90 min at 4°C. Fractions were collected using a Brandel Fraction Collector System. RNA was extracted from each fraction using Trizol reagent according to the manufacturer's protocol.

### Metabolic labeling and cell viability

Cells were incubated with complete growth media supplementing with EasyTagTM Express Protein Labeling Mix containing both [$^{35}$S]-L-methionine and [$^{35}$S]-L-cysteine (PerkinElmer) at 10 μCi/ml for 30 min at 37°C, 5% $CO_2$. Cells were then lysed in radioimmunoprecipitation assay (RIPA) buffer (150 mM NaCl, 1.0% IGEPAL-CA-630, 0.5% sodium deoxycholate, 0.1% SDS, 50 mM Tris, pH 8.0). Proteins were then separated on SDS-PAGE and transferred to a nitrocellulose membrane, followed by exposure to autoradiography films. Cell viability was measured 48 hours post-infection using the Cell Proliferation Kit I – MTT (Roche) according to the manufacturer's manual.

### Ribosome profiling

Ribosome profiling was performed as previously described on 2 biological replicates (Jafarnejad et al., 2018). Briefly, polysomes in 4T1 lysates were stabilized with cycloheximide and 4T1 lysates were split into two parallel workflows. RNA-Seq on total RNA from one half of the lysate (see below) while RNase I footprinting was performed on the remaining half to capture RPFs. For RNA-Seq, 150 μg of total RNA was taken for RNA-Seq analysis and Poly-(A)+ mRNA was purified using magnetic oligo-dT DynaBeads (Thermofisher) according to the manufacturer's instructions. Purified RNA was eluted and mixed with an equal volume of 2X alkaline fragmentation solution (2 mM EDTA, 10 mM $Na_2CO_3$, 90 mM $NaHCO_3$) and incubated for 20 min at 95°C. Fragmentation reactions were mixed with stop/precipitation solution (300 mM NaOAc pH 5.5 and GlycoBlue), followed by isopropanol precipitation by standard methods. Fragmented mRNA samples were size-selected on a denaturing 10% urea-polyacrylamide gel. The area corresponding to 35-50 nucleotides was excised, eluted and precipitated with isopropanol. Isolated RPF RNA (corresponding to 28-32 nt fragments) and total RNA fragments were used to create cDNA libraries as previously described (Jafarnejad et al., 2018). Ribosomal RNA (rRNA) contamination was reduced by subtractive hybridization using biotinylated oligos that were reverse complements of abundant rRNAs. The mRNA and ribosome-footprint libraries were then amplified by PCR (10 cycles) using indexed primers and sequenced on the Illumina HiSeq 2000 platform with read length of 50 nucleotides at the McGill University and Génome Québec Innovation Centre.

### Mapping and analysis of ribosome profiling data

The adaptor sequence was removed from reads using FASTX (Gordon, 2010) and reads that mapped to rDNA sequence by Bowtie 2 (Langmead and Salzberg, 2012) were discarded. Reads were then mapped to the mouse genome (mm9) using Bowtie 2. Uniquely mapped reads with MAPQ score $\geq$ 10 were used for further analysis. For gene expression analysis, reads mapping to the coding region of RefSeq transcripts were used to calculate Reads Per Kilobase per Million total uniquely mapped reads (RPKM). Gene-level RPKMs were obtained by conflating and averaging transcript RPKMs. Genes that showed no expression (0 RPKM) at either the transcription or translation levels in either the mock or infected samples were omitted from further analysis. Translation efficiency was defined by the $\log_2$ ratio of RPF to total RNA RPKMs. For metagene analysis of read distribution around start and stop codons, reads mapped to RefSeq transcripts were used. For a given region, only genes with at least 128 reads whose 5′ end was within the region were used. The 5′ end position of a read was used for the plotting. Subsets of differentially-expressed genes that are common and unique between the three oncolytic viruses were compiled using Venny v2.1 (Oliveros, 2007).

### Functional analysis of DEGs

Differentially-expressed genes that were commonly up- or downregulated in all three virus infections were tested for enrichment ($q < 0.10$) in Gene Ontology (GO) terms using BiNGO (GO terms downloaded October, 2015) (Maere et al., 2005). GO networks were plotted with the Enrichment Map plugin within Cytoscape 3.0 (Shannon et al., 2003). The "R" software package in the RStudio environment or GraphPad Prism was used for all other data manipulation and plotting. For sequence and RNA binding protein analyses, 5′ leaders and 3′ UTRs annotated in RefSeq were retrieved from UCSC Tables.

### Immunocytochemistry

4T1 cells were cultured as indicated on a 10 mm, #1.5 glass coverslip (Electron Microscopy Science). For intracellular staining, cells were washed with ice cold PBS followed by fixation in 4% paraformaldehyde in PHEM buffer (60 mM PIPES, 25 mM HEPES, pH6.9, 10 mM EGTA, 2 mM $MgSO_4$) for 10 min at room temperature. Fixed cells were treated with 50 mM $NH_4Cl$ in PBS to reduce autofluorescence, followed by permeabilization with 0.1% Triton X-100 in PBS for 10 min. Following 3 washes with PBS, the coverslip was then blocked with 5% BSA in PBS, for 30 min. Permeabilized cells were then incubated with the indicated primary antibody in 1% BSA/PBS overnight. Coverslips were washed 3 times for 5 min each with PBS and incubated with 1:10,000 dilution Goat anti-Rabbit IgG (H+L) Highly Cross-Adsorbed Secondary Antibody Alexa Fluor 568 secondary antibody (#A-11036, Invitrogen) for 1 hour at room temperature in the dark. Coverslips were washed 3 × 5 min with PBS and nuclei were stained with 1:200 of NucBlue® Live Ready Probe-variant of Hoechst dye (Life Technologies) in PBS for 5 min. Coverslips were then mounted onto slides using Prolong® Diamond mounting medium (Life Technologies). Confocal imaging was performed using a FV-1000 confocal microscope (Olympus) with a PlanApo N 100X/1.40 oil immersion objective lens (Olympus). Non-confocal fluorescence imaging was performed using an EVOS FL Cell Imaging system (Thermofisher). The following primary antibodies and corresponding dilution are used: 1:100 α-INPP5E (# ab69696, Abcam).

### Western blotting

Cells were washed with PBS and lysed in RIPA buffer supplemented with 10 mM NaF, 10 mM $Na_2VO_3$ and cOmplete Protease Inhibitor Cocktail (Roche). Cell debris was removed by centrifugation at 10,000 x *g*, 10 min, 4°C. Protein concentration of the supernatant was quantified using DC Protein assay (BioRad). Indicated amount of total protein was then loaded onto 10% SDS-polyacrylamide gel and separated by electrophoresis. Separated proteins were transferred to a nitrocellulose or PVDF membrane, then blocked with 5% skim milk in TBS-T buffer (10 mM Tris, 50 mM NaCl, 0.1% Tween-20, pH 7.5). The following primary antibodies and corresponding dilution were used: 1:500 α-INPP5E (#CPA3073, Cohesion Biosciences), 1:10,000 α-β-actin (#A5441, Sigma), 1:5000 α-GAPDH (#ab8245, Abcam), 1:2000 α-pan-HSV1 (#B011402, Dako), 1:2000 α-HSV1-ICP0 (#11060, Santa Cruz).

### Quantitative RT-PCR (RT-qPCR) and Droplet Digital RT-PCR (RT-ddPCR)

cDNA was reverse transcribed from total RNA using iScript Advanced cDNA Synthesis Kit (BioRad) according to the manufacturer's protocol. RT-qPCR was performed on cDNA mixed with iQ SyBR Green mix (BioRad) according to the manufacturer's protocol, using a Realplex 2 thermocycler (Eppendorf). The PCR conditions were 95°C for 3 min, followed by 40 cycles of 95°C for 10 s, 60°C for 30 s and 72°C for 30 s. Ct threshold was determined by Realplex software (Eppendorf). For calculating mRNA abundance, the ΔΔCt method relative to *Rps20* expression was used. For calculating short *Inpp5e* variant ratio, the ΔΔCt method relative to total *Inpp5e* expression was used. For the binding assays, RT-qPCR was performed directly on the extracted DNA using the same mix and PCR conditions as in qPCR assays, then the number of HSV1 genome relative to the number of host genome was calculated using the ΔΔCt method comparing relative abundance between HSV1 *UL30* and mouse *Lmnb2* abundance. For RT-ddPCR, cDNA was mixed with QX200 ddPCR EvaGreen Supermix (Biorad) according to the manufacturer's protocol and droplets were prepared using QX200 droplet generation oil on a QX200 Droplet Generator (Biorad). Droplets were subjected to PCR using a C1000 thermocycler (BioRad) using the cycling conditions: 95°C for 5 min, followed by 45 cycles of 95°C for 30 s at a ramp rate of 2°C/s and 60°C for 1 min at a ramp rate of 2°C/s. Positive/negative droplets were counted by a QX200 Droplet Reader (BioRad). Primers (listed 5′ to 3′) used for qPCR and ddPCR are listed in Table S4. For the gel-based assessment of 5′ leader expression, PCR was performed on 4T1 cDNA libraries using INPP5Eutr-F: CAGTCGTTGTTCCAGCTGC and INPP5E-shortUTR-R: TGAAAACTCGAGTGGCTCCC. For normalization of the CAT RNA reporter assay (see below), CAT cDNA was amplified using the above-noted ddPCR conditions with previously published primers (Riley et al., 2010). Melting curves and agarose electrophoresis were performed to control for PCR specificity in all of the above assays.

### CAT translation reporter assays

The CAT assay has been described previously (Graber et al., 2010). Briefly, 4T1, CT2A or MEFs were seeded at 3 or $6x10^5$ cells/well in 6-well plates, then co-transfected with 1 μg each of β-Galactosidase- (pBGal, obtained from Dr. Martin Holcik) and CAT-expressing plasmids using Lipofectamine 2000. 24 hours post-transfection, cells were lysed, and CAT expression was quantified using the CAT ELISA (Roche) as per the manufacturer's instructions. β-Galactosidase activity was measured using an ortho-Nitrophenyl-β-galactoside (ONPG) colorimetric assay. In the case of RNA transfection experiments, a T7-flanked long *Inpp5e* 5′ leader was amplified from 1 ng of the appropriate CAT reporter plasmid. This amplicon was used as a template for synthesis of capped and poly(A)-tailed RNA

using the T7 HiScribe *in vitro* transcription kit (New England Biolabs) according to the manufacturer's protocol. 1 μg of RNA was transfected with 2 μL of Lipofectamine 2000, and at 4 hours HSV1 was added into the media at indicated MOIs and incubated for an additional 18 hours. Cells were lysed in 300 μL of CAT lysis buffer, and 30 μL was used to isolate total RNA and prepare cDNA using iScript RT (BioRad). CAT cDNA was amplified by ddPCR using the above-noted primers and conditions. CAT expression was determined as above and normalized to the CAT RNA levels.

### CRISPR/Cas9-mediated gene knockout

CRISPR/Cas9 knockout of INPP5E in 4T1 was performed as previously described (Sanjana et al., 2014). Briefly, small guide RNAs (sgRNA) targeting the *Inpp5e* first exon or non-targeting sgRNA (primer sequences in Table S4) were cloned into the lenti-sgRNA(MS2)-zeomycin backbone (Addgene #61427) using BsmBI. To produce separate Cas9- and sgRNA-expressing lentiviruses, doxycycline-inducible and puromycin expressing pCW-Cas9 (Addgene #50661) or the constitutively expressing sgRNA vector were co-transfected with pLP1, pLP2 and pLP/VSVG (Thermofisher) into HEK293T cells using Lipofectamine 2000 (Invitrogen) according to the manufacturer's protocol. Cells were then transduced with the lentiviral supernatants and double-transductants were selected using puromycin and zeomycin. Cas9 expression was then induced using 1 μg/ml doxycycline for 24 hours. Single-cell clones were obtained by limiting dilution, screened using T7 Endonuclease I (New England Biolabs), and confirmed by Sanger sequencing. CRISPR/Cas9 modification efficiency was quantitated using TIDE, which deduces the frequency of individual insertion-deletion (indel) from Sanger sequencing of a mixed population.

### Live cell monitoring of virus spread

Live cells monitoring of virus infection was performed using the IncuCyte Live-Cell Analysis system (Sartorius). Cells were seeded in a 24-well plated at 80% confluency, then infected with viruses at the indicated MOI. Multiple phase contrast and fluorescence images were taken per well every 2 hours. Images were then analyzed using the IncuCyte Zoom software (Sartorius) for GFP cluster integrated intensity (Green calibrated unit x $\mu m^2$) as a measurement for virus infection. GFP cluster integrated intensity was calculated using the following customized process definition in Incucyte ZOOM software: background subtraction using Top-Hat method (disk shape structuring element with radius of 10 μm, threshold of 1.0 green calibrated unit), edge split: Off, Hole Fill: No, Adjust Size: No, Filters: No.

### Plaque assays

For titration, Vero cells were cultured to a monolayer. Cells were then incubated with a serial dilution in DMEM of virus-containing supernatant for 1 hours, 37°C, 5% $CO_2$ with shaking every 10 min. Cells were then washed 3 times with DMEM, then a layer of DMEM + 10% FBS +1% agar was added on top and allowed to solidify. Cells were then cultured at 37°C, 5% $CO_2$ for 48 hours (VSVΔ51) or 72 hours (HSV1, VACV). Full-well fluorescence images were taken, and fluorescent plaques were counted and used for back calculating original viral titer. For modified plaque assay to compare viral entry and spread (Figure 6D), monolayers of 4T1 WT or 4T1 Inpp5e$^{CRISPR}$ were cultured, then incubated virus diluted in RPMI media at a MOI of 0.01. Cells were then washed 3 times with RPMI media, then a layer of RPMI + 10% FBS +1% agar was added on top and allowed to solidify. Cell culture, and plaque detection and counting were carried out as described above for standard plaque assays.

### Binding assays

The cold binding assay was adapted for HSV1 from a previously described method (Abernathy et al., 2014). Briefly, cells were pre-incubated at 4°C for 30 min, then incubated with HSV1-1716 at the indicated MOI at 4°C for 1 hour. For internalization, cells were incubated for 1 hour at 37°C, washed with PBS pH 3.0 to remove surface bound viruses. gDNA was harvested using the QIAamp DNA Mini Kit (QIAGEN) according to manufacturer's protocol. PCR was performed using primers described above on the DNA.

## QUANTIFICATION AND STATISTICAL ANALYSES

All experiments were performed with at least 3 biological replicates unless otherwise specified in figure legends. Statistical significance was *a priori* set to 0.05. Two-tailed Student's t test or one-way ANOVA with Dunett's post hoc tests were performed where applicable unless otherwise indicated in the figure legend. Error bars indicate standard error of the mean (sem). *$p < 0.05$, **$p < 0.01$, ***$p < 0.001$, ****$p < 0.0001$, ns, non-significant.

## DATA AND CODE AVAILABILITY

Raw sequence files have been deposited on the NCBI Gene Expression Omnibus (GEO: GSE137757).